의학박사 학위논문

Role of ^{18}F-FEDAC PET as a TSPO-target imaging of activated macrophages in animal model of rheumatoid arthritis

류마티스 관절염 동물 모델에서 활성 대식세포 TSPO 표적 영상법으로서 ^{18}F-FEDAC PET 의 역할

2019 년 02 월

서울대학교 대학원

협동과정 종양생물학 전공

정 석 진

A thesis of the Doctor's degree

류마티스 관절염 동물 모델에서 활성 대식세포 TSPO 표적 영상법으로서 ^{18}F-FEDAC PET 의 역할

Role of ^{18}F-FEDAC PET as a TSPO-target imaging of activated macrophages in animal model of rheumatoid arthritis

February 2019

Interdisciplinary Program in Tumor Biology,
Seoul National University
College of Medicine
Seock-Jin Chung

류마티스 관절염 동물 모델에서 활성 대식세포 TSPO 표적 영상법으로서 ^{18}F-FEDAC PET 의 역할

지도교수 천 기 정

이 논문을 의학박사 박사학위논문으로 제출함

2019 년 02 월

서울대학교 대학원

협동과정 종양생물학 전공

정 석 진

정석진의 박사학위논문을 인준함

2019 년 02 월

위 원 장 _____ (인)

부 위 원 장 _____ (인)

위 원 _____ (인)

위 원 _____ (인)

위 원 _____ (인)

Role of ^{18}F-FEDAC PET as a TSPO-target imaging of activated macrophages in animal model of rheumatoid arthritis

by

Seock-Jin Chung

A Thesis Submitted to the Interdisciplinary Program

in Partial Fulfillment of the Requirements

for the Degree of Doctor of Philosophy

in Cancer Biology at the Seoul National University

February 2019

Approved by Thesis Committee:

Professor _____ **Chairman**

Professor _____ **Vice chairman**

Professor _____

Professor _____

Professor _____

ABSTRACT

Seock-Jin Chung

Interdisciplinary Program in Tumor Biology

The Graduate School

Seoul National University

Introduction: Rheumatoid arthritis (RA) is a chronic inflammatory joint disease resulting in destruction of multiple articular cartilages and bones. Activated macrophages play a pivotal role during the disease course and have been one of main targets to inhibit inflammatory reaction of RA by using biological disease-modifying anti-rheumatic drugs (bDMARDs). ^{18}F-FEDAC is one of PET imaging agents targeting TSPO, which is overexpressed in activated macrophages. In our previous study, we found that TSPO targeting PET ligand (^{18}F-FEDAC) can detect and image activated macrophages in animal model of RA. In this study, we evaluated the roles of ^{18}F-FEDAC monitoring the therapeutic effect of RA using TNF-antagonist (bDMARDs).

Materials & Methods: RAW 264.7 cells were activated with LPS and IFN-γ. After then, etanercept (ETN) and methotrexate (MTX) were incubated with the activated cells. Expressions of TSPO and glucose metabolism parameters (GLUT-1 and hexokinase-II) were measured using western blotting and immunofluorescence staining. Uptakes of ^{18}F-FEDAC and ^{18}F-FDG were evaluated in activated RAW 264.7 cells after ETN or MTX treatment. *In vivo* model of RA (collagen-induced arthritis; CIA) was established by intradermal injection of emulsified adjuvant and type II collagen in DBA1 mice. After ETN, MTX or vehicle treatments, ^{18}F-FEDAC and ^{18}F-FDG PET scans were performed. Two weeks after treatments, mice were sacrificed and immunostainings were performed in tissues of arthritic joints.

Results: Optimal concentrations of ETN (10 μg/ml) and MTX (5 nM) were determined by CCK-8 assay in activated RAW 264.7 cells. In *in vitro* study, expressions of TSPO and glucose metabolism parameters increased after activation, but did not change further after the treatment of ETN or MTX. Similarly, cellular uptake of both ^{18}F-FEDAC and ^{18}F-FDG increased after the

activation, but there were no uptake changes further after ETN or MTX treatments. In CIA mice, ^{18}F-FEDAC accumulation did not change during the ETN or MTX treatment. In contrast, ^{18}F-FDG accumulation at CIA mice was decreased during ETN or MTX treatments. Immunostaining showed that the expression of TSPO, CD68 and GLUT-1 did not change in inflamed joints after either ETN or MTX treatments. However, the expression of hexokinase-II decreased in either joints of ETN or MTX treated CIA mice compared to those of control CIA mice.

Conclusion: ^{18}F-FEDAC PET can image inflamed joints *in vivo* by targeting overexpressed TSPO of activated macrophages in a mouse CIA model. However, ^{18}F-FEDAC PET had a limited role to evaluate the therapeutic response by ETN on account of the sustained TSPO expression of macrophages once after their activation. According to the characteristics of TSPO expression, ^{18}F-FEDAC PET may be used as a signature marker for activated macrophages during the course of rheumatoid arthritis, even after therapeutic interventions.

In contrast, ^{18}F-FDG PET may be expected as an imaging biomarker to monitor therapeutic response of RA.

Keywords: Rheumatoid arthritis, Macrophages, Biological DMARDs, Etanercept, Translocator protein (TSPO), FEDAC, FDG, PET

Student number: 2014-22028

CONTENTS

LIST OF TABLES AND FIGURES

LIST OF ABBREVIATIONS

RA, Rheumatoid arthritis

DMARDS, Disease-modifying anti-rheumatic drugs

ETN, Etanercept

MTX, Methotrexate

TNF, Tumor necrosis factor

PET, Positron emission tomography

TSPO, Translocator protein

FBS, Fetal Bovine Serum

CIA, Collagen-induced arthritis

LPS, Lipopolysaccharide

GLUT, Glucose transporter

S.D., Standard deviation

S.E.M., Standard error of the mean

INTRODUCTION

Rheumatoid arthritis (RA) is one of the autoimmune disease that affects 0.5-1.0% of the general population (1). RA, unlike degenerative osteoarthritis, is a systemic inflammatory disease which can lead to destruction of multiple articular cartilage and bone (2-4). RA patients suffer from joint pain, stiffness, and swelling induced by joint inflammation, resulting in progressive destruction of cartilage and bone in joints (5).

For treatment RA, pharmacologic approaches have relied on combinations of non-steroidal anti-inflammatory drugs (NSAIDs; e.g. aspirin, ibuprofen), analgesics, glucocorticoids (e.g. prednisone, methylprednisolone), and disease-modifying anti-rheumatic drugs (DMARDs) (6, 7). NSAIDs or glucocorticoids have been known to reduce symptoms and signs. However, DMARDs (e.g. methotrexate, hydroxychloroquine, sulfasalazine) have long-term action and slow down disease progress itself of rheumatoid arthritis. Therefore, DMARDs are important medications in severe state of RA.

Methotrexate (MTX) is one of the widely used DMARDs and its efficacy has been proven in numerous controlled clinical trials (8-10). Low-dose MTX has immunomodulatory function which effects on neutrophil and monocyte function (8, 11, 12). MTX has established safety profiles and a relatively low cost of between $30 and $900 monthly (13). However, some patients dose not respond to MTX (14).

The new types of DMARDs (biological DMARDs) have been developed on understanding of the pathogenesis of RA. Although the causes of RA remain unknown, various cells and cytokines are involved in development and amplification of the inflammatory response (15, 16). Biological DMARDs are engineered drugs that target specific inflammatory cells, cellular interactions, and cytokines that mediate RA-related tissue damage. Such drugs are designed to reduce the signs and symptoms of RA and slow disease progression (17).

Nowadays, several biological DMARDs are used in RA patients. The first biological DMARDs for RA, a tumor necrosis factor (TNF)-antagonist,

etanercept (ETN), was approved by the US Food and Drug Administration (FDA) in 1998. Since then, several agents have become commercially available such as the TNF antagonists, interleukin (IL)-1 inhibitors, T-cell co-stimulation blocker, and B-cell depleting agents. These drugs were approved for moderate to severe RA which was not responded to non-biological DMARDs (18, 19). However, high cost of biological DMARDs, ranged from $2000 to $5000 monthly, are burden for patients (13). Thus, monitoring of early therapeutic effect with biological DMARDs is important for preventing overuse, proper patient selection and personalized therapy.

The visualization of RA activity has been restricted to conventional radiography, helping to establish the diagnosis and, subsequently, to monitor the progression of disease (20). Conventional radiography with computerized tomography (CT) and ultrasonography (US) are widely used for RA evaluation (21). They clearly delineate bone erosions and joint space narrowing but has limited role in early stage of RA (22-24). Magnetic resonance (MR) imaging is also useful to detect bone erosions in early rheumatoid arthritis than

conventional radiography. MR imaging could identify bone erosions in patients with less than 6 months disease duration than conventional radiography (25-27). However, MR imaging has some limitations such as long examination time, high cost, strong magnetic disturbance by metallic implants and inability to assess osteoporosis (28). In addition, MR images are non-specific and require differentiation from other pathologies manifested by the same spectrum of changes (29).

Nuclear medicine imaging modalities, such as single photon emission computed tomography (SPECT) and positron emission tomography (PET) have advantages to image metabolic and functional changes (30, 31). Bone scintigraphy is using ^{99m}Tc labeled phosphonate compounds to diagnosis the RA patients in nuclear medicine imaging. They accumulates at the sites of early new bone formation as a compensatory response to bone destruction of inflammation (32). But in many cases, distinction between degenerative, inflammatory and metastatic bone processes may be difficult (32, 33). Various

radiotracers have been developed for inflammation imaging, targeting different biomarkers from inflammatory cells to angiogenesis (34).

2-[^{18}F]Fluoro-2-deoxy-D-glucose (^{18}F-FDG) is the most widely used PET tracer, which reflects glucose metabolism. ^{18}F-FDG PET imaging used for detection not only cancer but also inflammatory response. Activated immune cells increase uptake of ^{18}F-FDG, producing high accumulation at inflammation and infection sites (35, 36). In inflammatory conditions, glucose transporters increase by various stimuli such as cytokines and growth factors (37, 38). ^{18}F-FDG accumulation increases in macrophages, neutrophils, and granulation tissues (39). Therefore, ^{18}F-FDG PET scan provides functional information about the inflammatory reaction based on glucose metabolism. However, ^{18}F-FDG uptake is not specific for inflammation. For this reason, direct targeting of immune cells is needed for specific visualization of RA.

The 18-KDa translocator protein (TSPO), which formerly known as peripheral benzodiazepine receptor (PBR) in the 1970s, is one of the biomarkers for inflammatory cells. TSPO is mainly found at outer

mitochondrial membrane and composed of five transmembrane helices. The function of TSPO is known as translocator of cholesterol and regulates the rate of steroid synthesis (40). Recently, it is known that increased TSPO expression has been associated with an activated state of macrophages and microglia (41-44). PET studies with TSPO-target ligand were performed in many types of central nervous system disorders such as stroke, Alzheimer's disease and Parkinson's disease (45-47). Most of these studies used the first generation of TSPO targeting PET tracer, ^{11}C-labeled *(R)*-*N*-methyl-*N*-(1-methylpropyl)-1-(2-chlorophenyl) isoquinoline-3-carboxamide (^{11}C-*(R)*-PK11195). However, carbon-11 has short half-life, resulting in low clinical applicability. To solve this problem, some fluorine-18 labeled TSPO ligands have been developed such as ^{18}F-PK14105 (48), ^{18}F-PBR102 (49), ^{18}F-CB251 (50), and ^{18}F-PBR28 (51).

N-Benzyl-N-methyl-2-[7,8-dihydro-7-(2-18F-fluoroethyl)-8-oxo-2-phenyl-9H-purin-9-yl]acetamide (^{18}F-FEDAC) is one of the second-generation TSPO targeting ligand with high specificity (52). In preclinical

studies, Yui et al. used ^{18}F-FEDAC in a rat brain ischemia model and found its accumulation in the infarct areas (53). Also, ^{18}F-FEDAC showed more significant uptakes at an inflammed lung lesion than ^{11}C-*(R)*-PK11195 (54). In previous study, we found that ^{18}F-FEDAC visualized inflammation of arthritic joints in RA animal model by targeting TSPO expression in activated macrophages (Fig. 1). Also, ^{18}F-FEDAC uptake was found in the joints of CIA mice in early phase, although ^{18}F-FDG uptake was not found (Fig. 2, Table 1) (55).

The aim of this study

In this study, we evaluated the roles of TSPO target PET ligand (^{18}F-FEDAC) monitoring the therapeutic effect of RA. *In vitro* cell studies and RA mouse model were used to evaluate changes during TNF-antagonist (ETN) treatment. For this purpose, uptakes and uptake mechanism of ^{18}F-FEDAC were compared with ^{18}F-FDG. ETN effects were also compared with MTX.

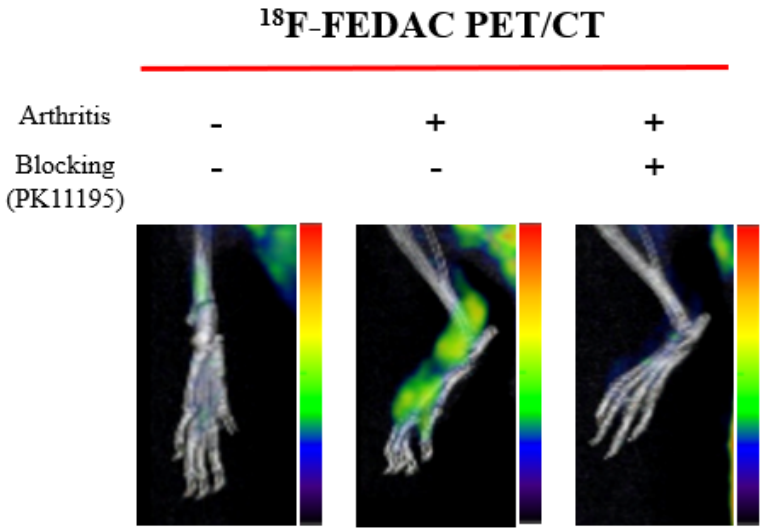

Figure 1. ^{18}F-FEDAC PET/CT images in normal and arthritis induced mice with or without cold form PK11195

Representative ^{18}F-FEDAC PET/CT images of both non-induced and arthritis induced (day 37) paws were shown. ^{18}F-FEDAC uptake in arthritic joint was higher than non-induced joint. ^{18}F-FEDAC uptake in arthritic joint was significantly decreased after blockage of TSPO by 1000-folds molar excess of nonradioactive PK11195.

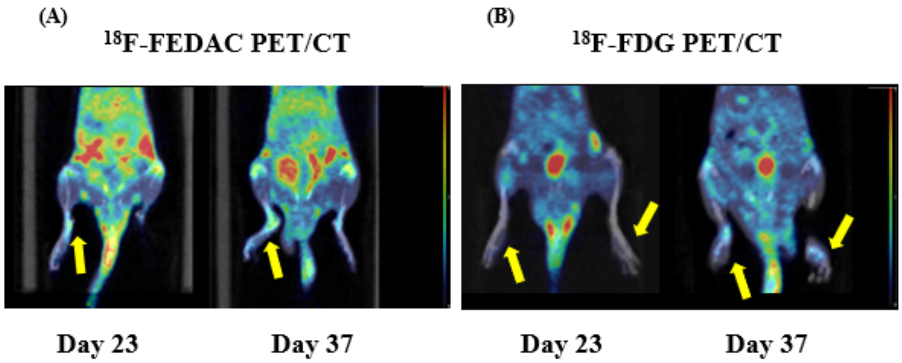

Figure 2. ^{18}F-FEDAC and ^{18}F-FDG PET/CT images in arthritis induced mice on early phase (day 23) and late phase (day 37)

(A) ^{18}F-FEDAC uptake of joints was found on both early phase (day 23) and late phase (day 37). (B) ^{18}F-FDG uptake of joints was not found on early phase (day 23). However, ^{18}F-FDG uptake of joints was found on late phase (day 37). Yellow allows indicated significant radiotracer uptake.

Table 1. TBR in normal and CIA mice

	Day 23			Day 37		
	Normal	**CIA**	**p value**	**Normal**	**CIA**	**p value**
^{18}F-FDG	0.17 ± 0.07	0.17 ± 0.05	0.859	0.28 ± 0.07	0.62 ± 0.27	<0.001*
^{18}F-FEDAC	0.22 ± 0.04	0.50 ± 0.16	<0.001*	0.18 ± 0.06	0.49 ± 0.27	<0.001*

*p<0.05
¶Time serial comparison of ^{18}F-FEDAC uptake in CIA group

Abbreviation: TBR, target to background ratio, CIA, collagen-induced arthritis, Statistical significance was determined by unpaired Student's t test. *p < 0.05. Data presented are the means ± s.d.

MATERIALS AND METHODS

Cell culture

Mouse macrophages cell line, RAW 264.7, was obtained from the American Type Culture Collection (ATCC, Manassas, VA, USA). RAW 264.7 cells were grown using DMEM culture medium (WelGene Inc., Daegu, South Korea) supplemented with 10 % fetal bovine serum (Invitrogen, Grand Island, NY, USA), 1% antibiotics (Invitrogen, Grand Island, NY, USA) in a 37℃ of humidified atmosphere containing at 5% CO_2. For macrophages activation, RAW 264.7 cells were treated with 200 ng/ml of lipopolysaccharide (LPS; Sigma-Aldrich, St. Louis, MO, USA) and 20 ng/ml of IFN-γ (Sigma-Aldrich, St. Louis, MO, USA) for 24 hr.

Cell viability test

Cell viability was confirmed using a cell counting kit-8 assay (CCK-8; Dojindo, Kumamoto, Japan). RAW 264.7 cells (1×10^3 cells/well) were

seeded in quintuplicate on 96-well plate and activated with LPS and IFN-γ for 24 hr. After then, either 0.1 to 100 μg/ml of ETN (Enbrel®; Pfizer, New York, NY, USA) or 5 to 25 nM of MTX (Sigma-Aldrich, St. Louis, MO, USA) were treated for 24 hr. The CCK-8 reagent 10 μL was added to each well, followed by incubation for an additional 4 hr, and the absorbance was measured at 450 nm using a Benchmark plus microplate reader (Bio-Rad Laboratories, Hercules, CA). The percentage of survival was calculated as follows: % survival = (mean absorbance in each group well/mean absorbance in control well) × 100.

Western blot analysis

RAW 264.7 cells (5×10^5 cells/well) were seeded on 6-well plate and activated with LPS and IFN-γ for 24hr. After then, either ETN (10 μg/ml) or MTX (5 nM) was treated for 0, 8, and 24 hr. In addition, 0.1 to 100 μg/ml of ETN were treated 24 hr for dose dependent study of ETN. Total proteins were isolated from RAW 264.7 cells using radio-immunoprecipitation assay (RIPA) buffer (Sigma-Aldrich, St. Louis, MO, USA) and protease inhibitor (Roche,

Nutley, NJ, Switzerland). Lysates of each sample (20 μg) were loaded onto 8% or 10% polyacrylamide gels. After electrophoresis, the gels were blotted onto PVDF membranes (Millipore, Watford, UK). The PVDF membranes were subjected to blocking with 5% skim milk or 5% BSA in Tris-Buffered Saline Tween-20 buffer (20 mM Tris, 137 mM NaCl and 0.1% Tween 20) for 1 hr at room temperature. The membranes were incubated overnight at 4℃ with primary antibody for inducible nitric oxidase synthase (iNOS; sc-651, Santa Cruz Biotechnology, CA, USA; diluted 1:300), TSPO (ab109497, Abcam, Cambridge, MA, USA; diluted 1:10000), hexokinase-II (#2867s, Cell Signaling Technology, Danvers, MA, USA; diluted 1:1000), GLUT-1 (ab64693, Abcam, Cambridge, MA, USA; diluted 1:500) and β-actin (A5451, Sigma-Aldrich, St. Louis, MO, USA); diluted 1:5000). Membrane were then probed with HRP conjugated anti-rabbit or anti-mouse IgG (Cell signaling Technology, Danvers, MA, USA). Visualization was performed using ECL reagents (Roche, Nutley, NJ, USA). The signal intensity was measured using ChemiDoc™ (Bio-Rad,

Hercules, CA, USA). The TSPO expression level of activated macrophage was compared with non-activated control.

Immunofluorescence staining in cells

For immunofluorescence staining, 5×10^3 RAW 264.7 cells were seeded in each 8-well chambered slide (Thermo Fisher Scientific, Waltham, MA, USA) with LPS and IFN-γ stimulation for 24 hr. After then, either ETN (10 μg/ml) or MTX (5 nM) was treated in stimulated cells additional 24hr. Each well was fixed with 4% paraformaldehyde for 10 min and permeabilized with 0.5% Triton X-100 for 5 min. RAW 264.7 cells were blocked with 5% BSA for 30 min and incubated with primary antibodies overnight at 4℃ as follows: anti-NF-κB (#8242, Cell Signaling Technology, Danvers, MA, USA; diluted 1:400), anti-TSPO (ab109497, Abcam, Cambridge, MA, USA; diluted 1:400), hexokinase-II (#2867s, Cell Signaling Technology, Danvers, MA, USA; diluted 1:200) and GLUT-1 (ab64693, Abcam, Cambridge, MA, USA; diluted 1:100). Cells were washed three times with PBS and stained with Alexa-647

labeled anti-rabbit antibody for 1hr in room temperature. After staining, cells were washed three times with PBS and mounted with Prolong Gold reagent (Invitrogen, Grand Island, NY, USA). Fluorescence images were acquired using Zeiss LSM 800 confocal imaging system (Carl Zeiss, Jena, Germany).

In vitro cell uptake assay

RAW 264.7 cells (1×10^4 cells/well) were seeded in quadruplicate on 24-well plate and activated with LPS and IFN-γ for 24hr. After then, either ETN (10 μg/ml) or MTX (5 nM) was treated for 0, 8, and 24 hr. Each well was washed with serum-free DMEM medium and incubated with the 5μCi of ^{18}F-FEDAC or ^{18}F-FDG in 500 μL of DMEM medium for 1hr at 37℃. Cells were washed two times with cold HBSS and lysis with 250 μL of 1% SDS. Radioactivity was measured by use of a 1470 automatic γ-counter (PerkinElmer, Waltham, MA, USA). Radioactivity was normalized with protein amount at the time of assay.

Induction of collagen-induced arthritis and drugs treatment

All experimental procedures were approved by the Institutional Animal Care and Use Committee of the Seoul National University (IACUC No. SNU-160718-7-5). We used collagen-induced arthritis (CIA) mouse model as a RA animal model. Total 20 mice (DBA1, Seven-week-old, male) were injected subcutaneously in the tail base region with 50 μL of bovine type II collagen (Chondrex, Redmond, WA, USA) emulsified in an equal volume of complete Freund's adjuvant (CFA). Three weeks after, the mice were injected in the similar region with 50 μL of bovine type II collagen emulsified with incomplete Freund's adjuvant (IFA) as a booster immunization. Since the second injection, the severity of the arthritis was scored as described previously [Nature Protocol. 2007] (56). An arthritis score of 0 indicates that no macroscopical evidence of erythema and swelling, 1 indicates that erythema and mild swelling confined to the tarsals, 2 indicates that erythema and mild swelling extending from the ankle to the tarsals, 3 indicates that erythema and

moderate swelling extending from the ankle to the tarsals, and 4 indicates that erythema and severe swelling encompass the ankle, foot and digits, or ankylosis of the limb. We checked CIA mice arthritis score every two days after second immunization. We selected mice which induced high arthritis scored (score 4) paw at least one site, and divided three groups: ETN (4 mice, 16 paws), MTX (4 mice, 16 paws) and saline (2 mice, 8 paws) treated groups. In addition, we divided arthritic paws into fully swollen paws (score 4) and non-fully swollen paws (lower than score 4) for analysis. Each group was given intraperitoneal injection of ETN (100 μg), MTX (0.5 mg/kg) or vehicle (saline 100 μL) every two days. Treatments were lasted until 2 weeks. Delta arthritis score was calculated as the change of arthritis scores during treatment period (arthritis score after 14 days treatment – arthritis score pre-treatment).

PET imaging and analysis

PET scan was performed using a small animal PET scanner (simPET, Brightonic imaging, Seoul, Korea). ^{18}F-FEDAC and ^{18}F-FDG PET scans were

performed at the same CIA mice pre-treatment of ETN, MTX or vehicle. Follow-up PET scans were performed once a week until two weeks after ETN, MTX or vehicle treatment. Anesthesized mice with 1.5% isofluorane were injected radiotracers (14.1±0.8 MBq/0.1 ml for ^{18}F-FEDAC, 15.5±0.5 MBq/0.2 ml for ^{18}F-FDG) and took PET scans 10 minutes at 1 hr after injection of radiotracers. Images were reconstructed using a three-dimensional ordered-subset expectation maximization (3D OSEM) algorithm. PET images were converted into DICOM files and were analyzed using AMIDE software. The maximal standardized uptake value (SUV_{max}) was measured using volume of interests (VOIs) which placed on the CIA mice joints. The SUV_{max} was calculated in a pixel as (tissue radioactivity concentration)/[(injected radioactivity)/(body weight)]. The blood-pool SUV_{max} was measured from the thoracic aorta for normalization; thereby, a target-to-background ratio (TBR) value was acquired for each subject.

Immunohistochemistry analysis in tissues

Paws (*n = 3*) of ETN, MTX or vehicle treated group were amputated and fixed in 10 % paraformaldehyde for seven days at room temperature. Bone tissues were decalcified for about 1 weeks at 4 °C in a solution with 14 % ethylenediaminetetraacetic acid (EDTA, Sigma-Aldrich, St Louis, MO, USA) (pH 7.2). After decalcification, joints were washed and prepared for paraffin embedding. Sagittal sections (4 μm) from the center of joint were used for slides. For staining, dehydrated sections were permeabilized in 0.5% Triton X-100 for 5 min. The sections were blocked with goat or horse serum (diluted 1:30 in PBS) for 1hr at room temperature. The slides were incubated overnight with primary antibodies for TSPO (ab109497, Abcam, Cambridge, MA, USA; diluted 1:200), CD68 (sc-7089, Santa Cruz Biotechnology, CA, USA; diluted 1:200), hexokinase-II (#2867s, Cell Signaling Technology, Danvers, MA, USA; diluted 1:200) and GLUT-1 (ab64693, Abcam, Cambridge, MA, USA; diluted 1:100) at 4℃. After washing with PBS, biotinylated secondary antibodies were incubated 1hr at room temperature. After staining, samples were amplified with a complex of avidin-biotin peroxidase, and developed using DAB. Then,

samples were counterstained with hematoxylin. Images were observed using a light microscope (BX43, Olympus, Center Valley, PA, USA).

Statistical analysis

All statistical analyses were performed using GraphPad Prism's statistical analysis and MedCalc program. The Mann-Whitney test was used to determine the statistical significances of cell viability, cell uptake assay and PET analysis. The Kruskal-Wallis test was used to determine the difference of clinical courses among ETN, MTX and vehicle treatment. After then, post-hoc analysis was performed to find difference of mean values among groups. *P* values < 0.05 were considered statistically significant.

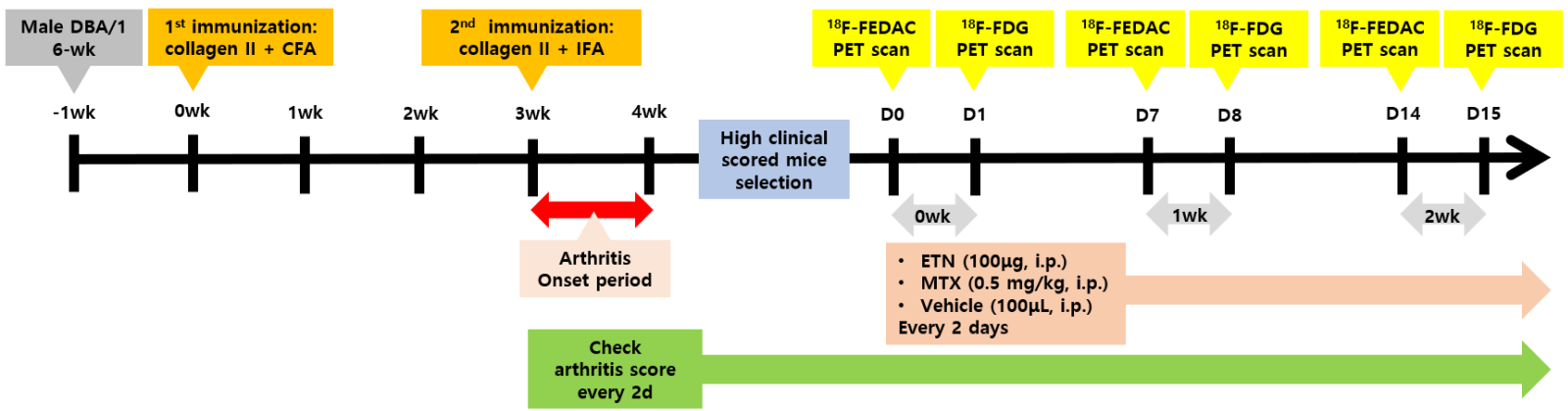
Male DBA/1
6-wk
1st immunization:
collagen II + CFA
2nd immunization:
collagen II + IFA
18F-FEDAC
PET scan
18F-FDG
PET scan
18F-FEDAC
PET scan
18F-FDG
PET scan
18F-FEDAC
PET scan
18F-FDG
PET scan
-1wk
0wk
1wk
2wk
3wk
4wk
High clinical
scored mice
selection
D0
D1
D7
D8
D14
D15
0wk
1wk
2wk
Arthritis
Onset period
• ETN (100μg, i.p.)
• MTX (0.5 mg/kg, i.p.)
• Vehicle (100μL, i.p.)
Every 2 days
Check
arthritis score
every 2d

Figure 3. CIA modeling scheme and *in vivo* study scheme

Emulsion with adjuvant and type II collagen was intradermally injected two times in DBA1 mice for CIA modeling. Among 20 CIA induced mice, we selected 10 mice which induced high arthritis score (score 4) of arthritis at least one paw. We separated 10 CIA mice into 3 groups; ETN treated group (4 mice), MTX treated group (4 mice), and vehicle treated group (2 mice). After PET scans were taken on 0 week (D0, D1), drugs (ETN, MTX and vehicle) were treated every 2 days in each group of CIA mice. For the follow-up study, PET images were obtained once a week until two weeks.

RESULTS

Cell viability test with ETN and MTX

In CCK-8 assays, cytotoxicity of ETN was not significantly affected to activated RAW 264.7 cells even if treated using high dose of ETN concentration (100 μg/ml) (Fig. 4a). Cytotoxicity of MTX was increased according to dose dependent, and more than half of activated RAW 264.7 cells were dead at 24 hr after 20 nM of MTX treatment (Fig. 4b). Based on this data, we selected 10 μg/ml of ETN (93.6% ± 8.2% survival rate) and 5 nM of MTX (91.4% ± 5.5% survival rate) for *in vitro* study which showed similar survival rate.

Confirmation of ETN effect in cellular level

In western blotting, we confirmed cell activation using the expression of iNOS, which is known as a marker of TNF-α dependent activation. The expression of iNOS was increased after activation compared to non-activated

RAW 264.7 cells. In activated RAW 264.7 cells, the expression of iNOS slightly decreased after ETN treatment for 24 hr. However, the expression of iNOS slightly increased after MTX treatment for 24 hr in activated RAW 264.7 cells (Fig 5a). The expression of iNOS did not change according to ETN concentration (0.1 to 100 μg/ml) in activated RAW 264.7 cells for 24 hr (Fig. 5b). In immunofluorescence results showed that translocations of NF-κB in nucleus increased after activation in RAW 264.7 cells. Translocations of NF-κB in nucleus decreased after 24hr ETN treatment. In contrast, translocations of NF-κB in nucleus did not change after 24 hr MTX treatment compared to normal activated RAW 264.7 cells (Fig. 5c).

Monitoring the expression of TSPO in cellular level after drugs treatment

The expression of TSPO in RAW 264.7 cells

In RAW 264.7 cells, the expression of TSPO increased after 24hr activation but did not changed further after ETN or MTX treatment in western blotting results (Fig. 6a). The expression of TSPO did not change according to ETN concentration (0.1 to 100 μg/ml) in activated RAW 264.7 cells for 24 hr (Fig. 6b). In immunofluorescence staining, the expression of TSPO increased after activation but didn't change at 24 hr further after either ETN or MTX treatment (Fig. 6c). Both western blotting and immunofluorescence results showed that the expression of TSPO increased after activation but neither ETN nor MTX affected the expression of TSPO in activated RAW 264.7 cells.

Cell uptake of ^{18}F-FEDAC in RAW 264.7 cells

^{18}F-FEDAC uptakes were 1.8-folds higher in activated RAW 264.7 cells than in non-activated RAW 264.7 cells. However, ^{18}F-FEDAC showed no significant uptake changes after ETN ($p = 0.0996$) or MTX ($p = 0.2704$) treatment (Fig. 7).

Monitoring the expression of glucose metabolism parameters in cellular level after drugs treatment

The expression of glucose metabolism parameters (GLUT-1 and hexokinase-II) in RAW 264.7 cells-

In western blotting, the expressions of GLUT-1 and hexokinase-II increased after activation compared to non-activated RAW 264.7 cells. However, the expressions of GLUT-1 and hexokinase-II did not change further after ETN or MTX treatment in western blotting results (Fig. 8a). In immunofluorescence staining, the expressions of GLUT-1 and hexokinase-II increased after activation but didn't change at 24 hr further after either ETN or MTX treatment (Fig. 8b). Both western blotting and immunofluorescence results showed that the expressions of GLUT-1 and hexokinase-II increased after activation but neither ETN nor MTX affected expression of glucose metabolism parameters in activated RAW 264.7 cells.

Cell uptake of ^{18}F-FDG in RAW 264.7 cells

^{18}F-FDG uptakes were 3-folds higher in activated RAW 264.7 cells than in non-activated RAW 264.7 cells. During the ETN treatment, ^{18}F-FDG uptake decreased by 14% at 24 hr after treatment compared to non-treated activated RAW 264.7 cells ($p = 0.0006$). In contrast, ^{18}F-FDG uptake did not decreased after MTX treatment ($p = 0.2632$) in activated RAW 264.7 cells (Fig. 9).

Monitoring therapeutic response in animal model of RA

Clinical course of CIA mice with ETN, MTX and vehicle treatment

The joint swelling appeared one week after the second immunization. Various patterns of increasing arthritis score were shown in CIA paws. Arthritis scores of paws decreased after ETN treatment compared to those of vehicle treatment (Fig. 10a). Delta arthritis score of ETN treated mice was lower than vehicle treated mice ($p = 0.0327$) (Fig. 10b).

We selected fully swollen paws (score 4) pre-treatment of drugs among ETN (8 paws), MTX (7 paws) and vehicle (5 paws) treated CIA mice.

Arthritis scores of fully swollen paws slightly decreased after ETN, MTX and vehicle treatment (Fig. 10c). Delta arthritis scores were not different among ETN, MTX and vehicle treated mice (Fig. 10d).

In non-fully swollen paws (lower than score 4), arthritis scores decreased after ETN treatment (8 paws) but did not change after MTX treatment (9 paws). In addition, arthritis scores significantly increased after vehicle treatment (3 paws) (Fig. 10e). Delta arthritis score of both ETN ($p = 0.0049$) and MTX ($p = 0.0083$) treated mice were lower than vehicle treated mice (Fig. 10f).

Monitoring therapeutic response with ^{18}F-FEDAC and ^{18}F-FDG PET scans in arthritic paws

To monitor activated macrophages in arthritic joints during the ETN, MTX or vehicle treatment, we scanned CIA mice once a week with ^{18}F-FEDAC and ^{18}F-FDG PET. High ^{18}F-FEDAC accumulation was found pre-treatment (0 week) in arthritic joints of CIA mice. ^{18}F-FEDAC PET uptakes of arthritic

joints did not decreased after either ETN or MTX treatment (Fig. 11). High ^{18}F-FDG accumulation was found pre-treatment (0 week) in arthritic joints of CIA mice. In contrast to ^{18}F-FEDAC, ^{18}F-FDG PET signals of arthritic joint significantly decreased after either ETN or MTX treatment. However, arthritic joints of vehicle treatment didn't decrease ^{18}F-FDG PET signals (Fig. 12).

In paws of CIA, arthritis scores slightly decreased during ETN (16 paws) or MTX (16 paws) treatment compared to vehicle (8 paws) treatment (Fig. 13a, b, c). TBR of ^{18}F-FEDAC after ETN, MTX or vehicle treatment didn't change during the therapy period (Fig. 13d, e, f). TBR of ^{18}F-FDG after ETN treatment decreased by 49% in the first week ($p = 0.0019$) and decreased by 66% in the second week ($p < 0.0001$) compared to those of pre-treatment (Fig. 13g). TBR of ^{18}F-FDG after MTX treatment decreased by 39% in the second week ($p = 0.0241$) compared to those of pre-treatment (Fig. 13h). TBR of ^{18}F-FDG after vehicle treatment did not change until the second week (Fig. 13i).

Monitoring therapeutic response with ^{18}F-FEDAC and ^{18}F-FDG PET scans in fully swollen paws

In the fully swollen paws, arthritis scores slightly decreased during ETN (8 paws), MTX (7 paws) and vehicle (5 paws) treatment (Fig. 14a, b, c). TBR of ^{18}F-FEDAC after ETN, MTX or vehicle treatment didn't change during the therapy period compared to those of pre-treatment (Fig. 14d, e, f). TBR of ^{18}F-FDG after ETN treatment decreased by 54% in the first week ($p = 0.003$) and decreased by 79% in the second week ($p = 0.0002$) compared to those of pre-treatment (Fig. 14g). TBR of ^{18}F-FDG after MTX treatment decreased by 40% ($p = 0.0379$) in the first week, and decreased ($p = 0.0973$) by 53% in the second week compared to those of pre-treatment (Fig. 14h). TBR of ^{18}F-FDG after vehicle treatment did not change until second week (Fig. 14i).

Monitoring therapeutic response with ^{18}F-FEDAC and ^{18}F-FDG PET scans in non-fully swollen paws

In non-fully swollen paws, arthritis scores decreased during ETN (8 paws) treatment. Arthritis scores didn't change during MTX (7 paws) treatment and significantly increased during vehicle (5 paws) treatment (Fig. 15a, b, c). TBR of ^{18}F-FEDAC after ETN, MTX or vehicle treatment didn't change their values during treatment compared to those of pre-treatment (Fig. 15d, e, f). TBR of ^{18}F-FDG after ETN treatment decreased by 36% in the first week ($p = 0.0249$) and decreased by 34% ($p = 0.019$) in the second week compared to those of pre-treatment (0 week) (Fig. 15g). TBR of ^{18}F-FDG after MTX treatment didn't change their values during treatment compared to those of pre-treatment (Fig. 15h). TBR of ^{18}F-FDG after vehicle treatment 2-folds increased ($p = 0.05$) at the second week of treatment compared to those of pre-treatment (Fig. 15i).

Expression of TSPO, GLUT-1 and hexokinase-II in arthritic paws after ETN, MTX and vehicle treatment

In H&E staining results, cell infiltration and bone destruction were found in arthritic joints of ETN, MTX and vehicle treatment. The expression of TSPO did not change in arthritic joint of ETN or MTX treatment compared to those of vehicle treatment. Also, the expression of CD68, which is known as monocyte/macrophages marker, colocalized with TSPO in arthritic joint tissues of ETN, MTX or vehicle treatment. The expression of GLUT-1 was found in arthritic joints of either ETN or MTX treatment, but hexokinase-II was less expressed in arthritic joints of either ETN or MTX treatment than vehicle treatment (Fig. 16).

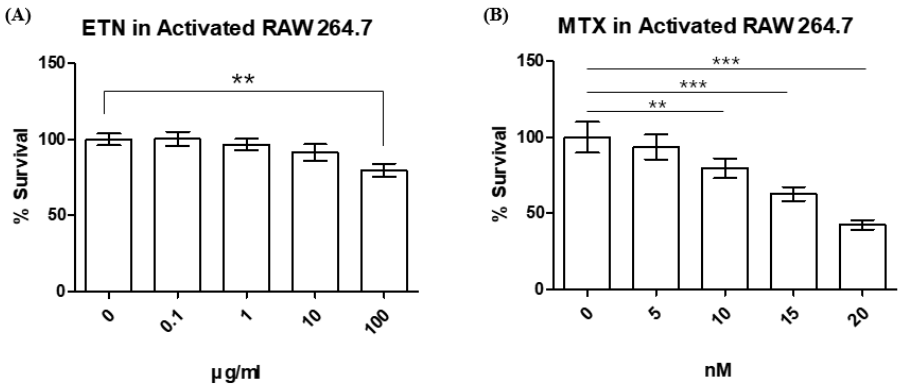

Figure 4. Cell viability test in activated RAW 264.7 cells

Cell viabilities in activated RAW 264.7 cells were measured by CCK-8 assay. (A) Cell viability of activated RAW 264.7 cells were not decreased until 100 μg/ml of ETN treatment for 24 hr. (B) Cell viability of activated RAW 264.7 cells were gradually decreased according to dose dependent of MTX treatment for 24 hr. From this data, both 10 μg/ml of ETN and 5 nM of MTX showed similar survival rate in activated RAW 264.7 cells. Statistical significance was determined by Mann-Whitney test. *$p < 0.05$, **$p < 0.005$, ***$p < 0.0005$. Data presented are the means ± s.d.

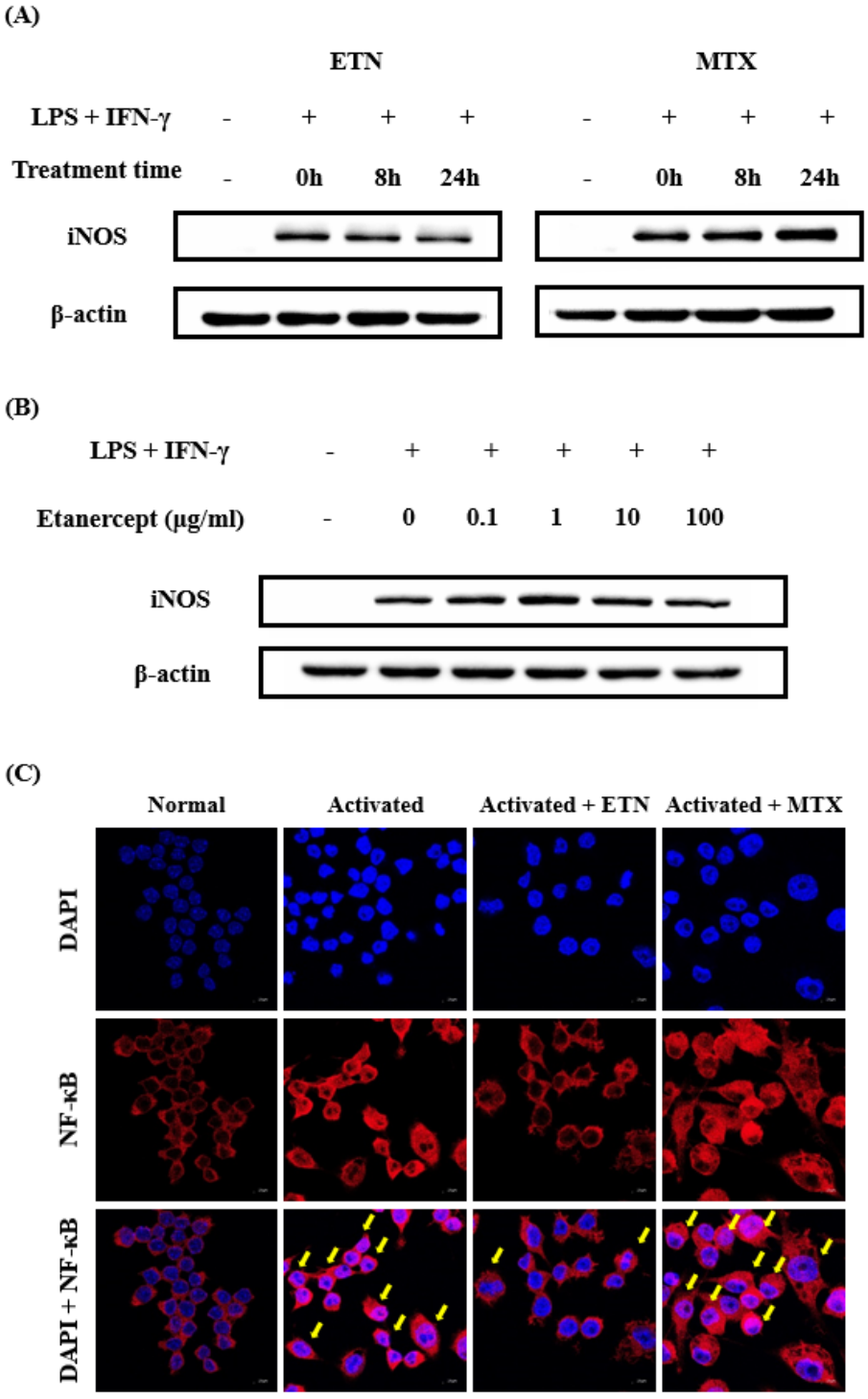
(A)
ETN
MTX
LPS + IFN-γ
- + + + - + + +
Treatment time
- 0h 8h 24h - 0h 8h 24h
iNOS
β-actin
(B)
LPS + IFN-γ
- + + + + +
Etanercept (μg/ml)
- 0 0.1 1 10 100
iNOS
β-actin
(C)
Normal
Activated
Activated + ETN
Activated + MTX
DAPI
NF-κB
DAPI + NF-κB

Figure 5. Confirmation of ETN effect in RAW 264.7 cells using western blotting and immunofluorescence imaging

(A) The expressions of iNOS (activation marker) was evaluated by western blotting. After activation with LPS and IFN-γ for 24hr, iNOS significantly increased compared to non-stimulation. The expression of iNOS slightly decreased after 24 hr ETN treatment. In contrast, the expression of iNOS slightly increased after 24 hr MTX treatment. (B) In activated RAW 264.7 cells, the expression of iNOS did not decrease after 24 hr treatment of ETN according to the concentration from 0 to 100 μg/ml. (C) Translocations of NF-κB in nucleus increased after activation with LPS and IFN-γ for 24hr compared to normal RAW 264.7 cells. In activated RAW 264.7 cells of ETN treatment, translocations of NF-κB in nucleus decreased after 24 hr treatment. In activated RAW 264.7 cells of MTX treatment, translocations of NF-κB in nucleus did not decrease after 24 hr treatment. Red signals show NF-κB and blue signals show DAPI staining. Yellow allows indicate translocation of NF-κB in nucleus.

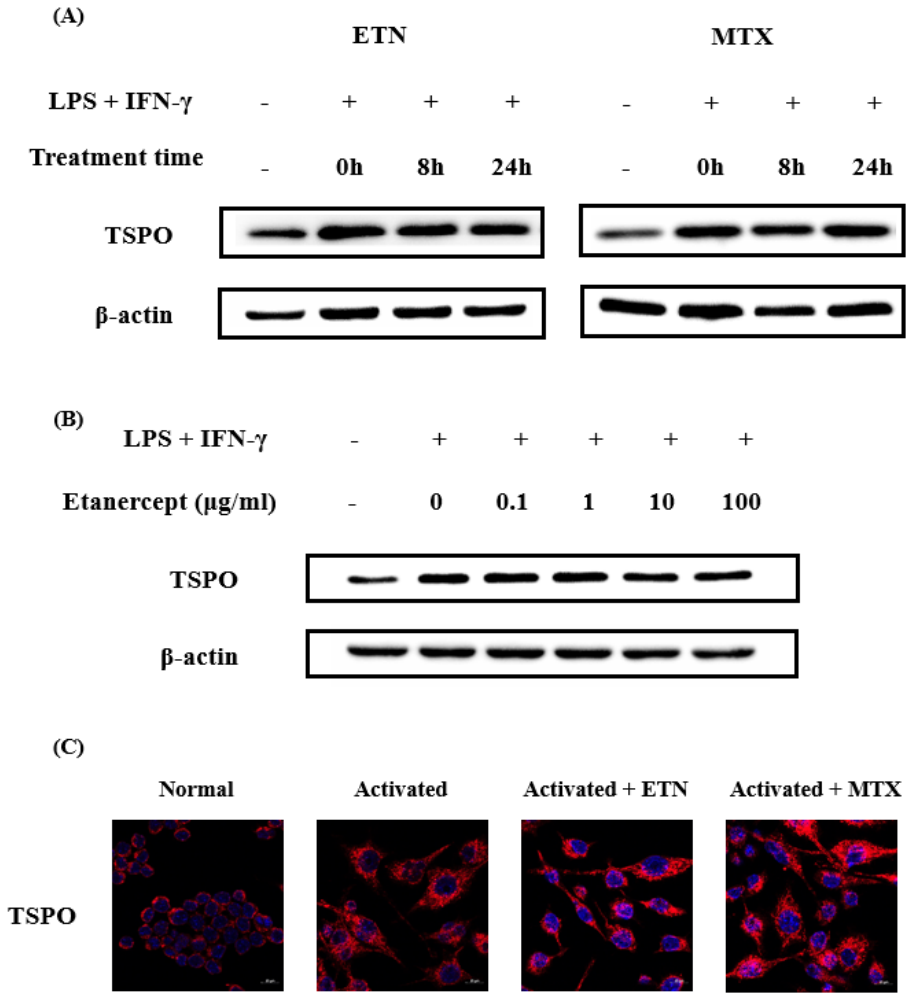
(A)
ETN
MTX
LPS + IFN-γ
- + + + - + + +
Treatment time
- 0h 8h 24h - 0h 8h 24h
TSPO
β-actin
(B)
LPS + IFN-γ
- + + + + +
Etanercept (μg/ml)
- 0 0.1 1 10 100
TSPO
β-actin
(C)
Normal
Activated
Activated + ETN
Activated + MTX
TSPO

Figure 6. The expression of TSPO in RAW 264.7 cells after ETN or MTX treatment

(A) The expression of TSPO was evaluated by western blotting. After activation with LPS and IFN-γ for 24hr, the expression of TSPO significantly increased compared to normal RAW 264.7 cells, but did not change further after ETN or MTX treatment. (B) In activated RAW 264.7 cells, the expression of TSPO did not change after 24 hr treatment of ETN according to the concentration from 0 to 100 μg/ml. (C) The expression of TSPO was evaluated by immunofluorescence imaging. The expression of TSPO increased in RAW 264.7 cells after activation compared to normal RAW 264.7 cells, but did not change further 24 hr after ETN or MTX treatment. Red signals show TSPO and blue signals show DAPI staining.

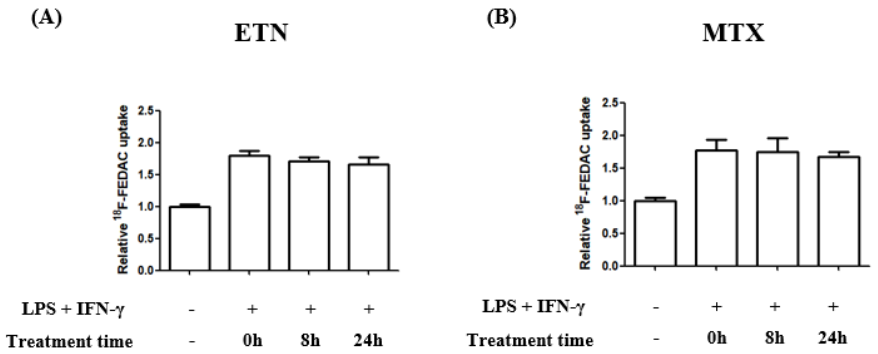

Figure 7. *In vitro* uptakes of ^{18}F-FEDAC in RAW 264.7 cells after ETN or MTX treatment

^{18}F-FEDAC uptake assays in cells were measured by radioactivity using a gamma counter. ^{18}F-FEDAC accumulation was 1.8-folds increased during the activation with LPS and IFN-γ for 24 hr. However, ^{18}F-FEDAC uptake did not change after either (A) ETN or (B) MTX treatment in activated RAW 264.7 cells until 24 hr. Data presented are the means ± s.d.

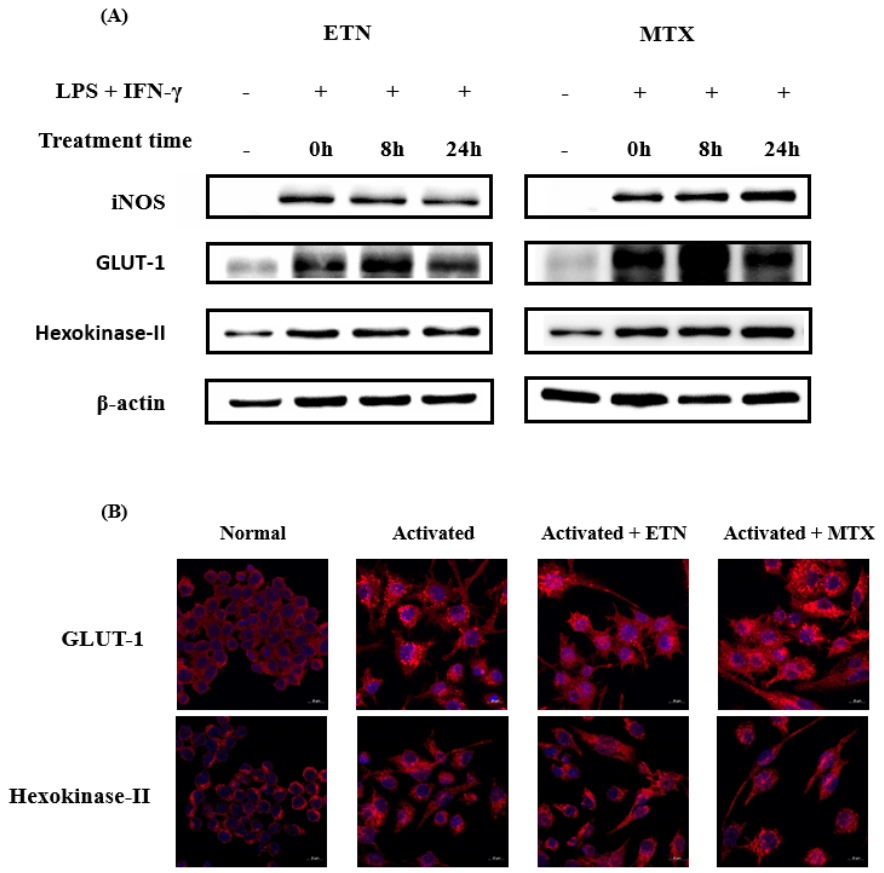

Figure 8. The expression of glucose metabolism parameters in RAW 264.7 cells after ETN or MTX treatment

(A) The expressions of glucose metabolism parameters (GLUT-1 and hexokinase-II) were evaluated by western blotting. After activation with LPS and IFN-γ for 24hr, the expressions of GLUT-1 and hexokinase-II increased after stimulation, but did not significantly change further after ETN or MTX treatment. (B) The expressions of GLUT-1 and hexokinase-II were evaluated by immunofluorescence imaging. The expressions of GLUT-1 and hexokinase-II increased in RAW 264.7 cells after activation, but did not change further 24 hr after ETN or MTX treatment. Red signals show GLUT-1 and hexokinase-II expression and blue signals show DAPI staining.

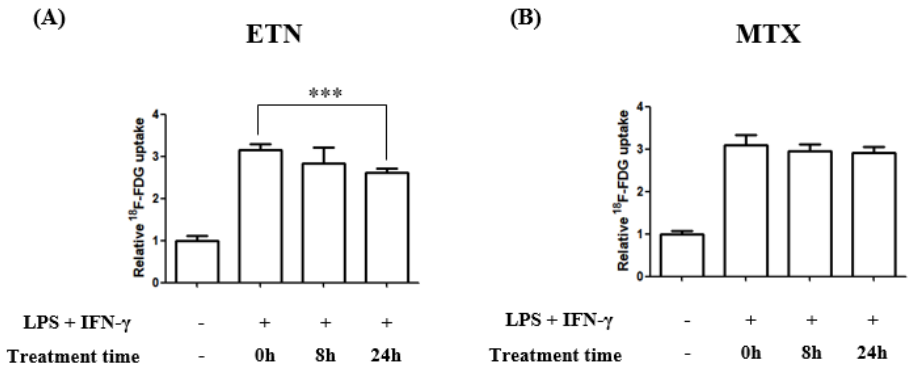

Figure 9. *In vitro* uptakes of ^{18}F-FDG in RAW 264.7 cells after ETN or MTX treatment

^{18}F-FDG uptake assays in cells were measured by radioactivity using a gamma counter. ^{18}F-FDG accumulation was 3-folds increased during the activation with LPS and IFN-γ for 24 hr. (A) In activated RAW 264.7 cells, ^{18}F-FDG uptake 14% decreased at 24h after ETN treatment. (B) However, ^{18}F-FDG uptake did not change in activated RAW 264.7 cells after MTX treatment. Statistical significance was determined by Mann-Whitney test. *$p < 0.05$, **$p < 0.005$, ***$p < 0.0005$. Data presented are the means ± s.d.

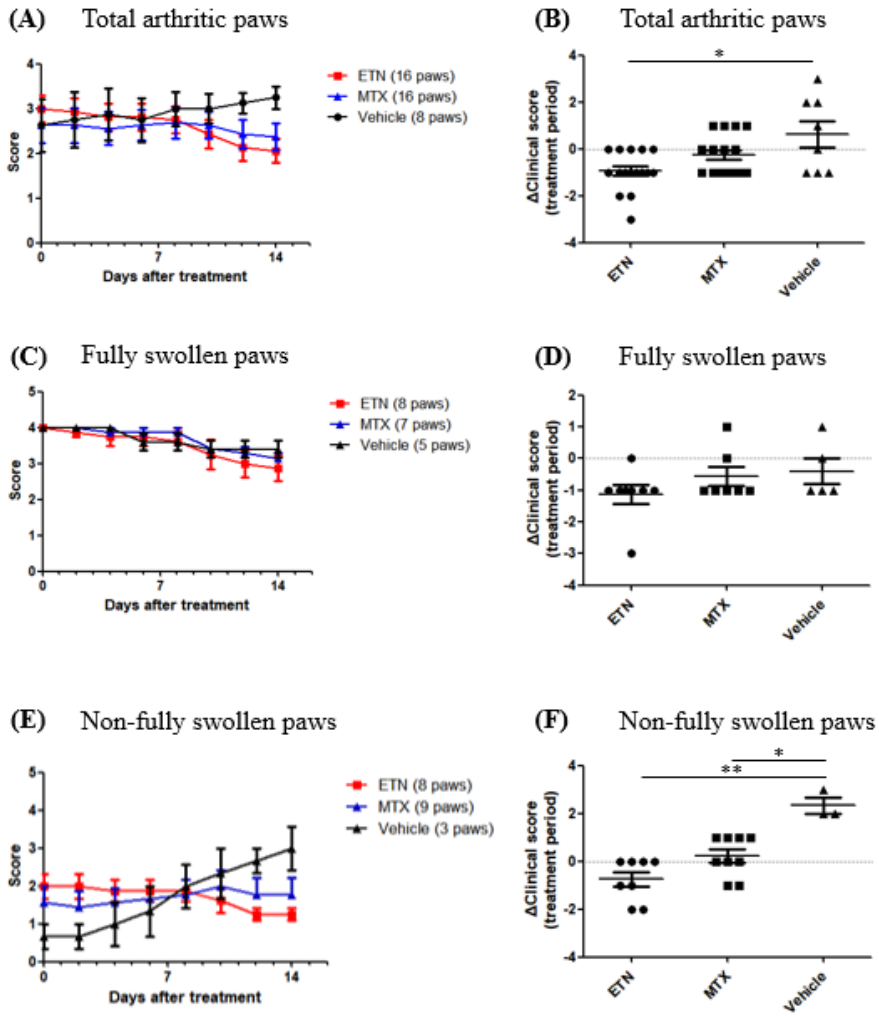
(A) Total arthritic paws
ETN (16 paws)
MTX (16 paws)
Vehicle (8 paws)
Score
Days after treatment
(B) Total arthritic paws
*
ΔClinical score (treatment period)
ETN
MTX
Vehicle
(C) Fully swollen paws
ETN (8 paws)
MTX (7 paws)
Vehicle (5 paws)
Score
Days after treatment
(D) Fully swollen paws
ΔClinical score (treatment period)
ETN
MTX
Vehicle
(E) Non-fully swollen paws
ETN (8 paws)
MTX (9 paws)
Vehicle (3 paws)
Score
Days after treatment
(F) Non-fully swollen paws
*
**
ΔClinical score (treatment period)
ETN
MTX
Vehicle

Figure 10. The clinical course of CIA mice after ETN, MTX or vehicle treatment and graphs of delta arthritis score

(A) In arthritis scores results, paws of ETN (16 paws) and MTX (16 paws) treatment decreased their arthritis scores during the treatment. However, paws of vehicle (8 paws) treatment increased their arthritis scores during the treatment. (B) Delta arthritis score value of ETN treated paws was lower than those of vehicle treated paws. (C) In fully swollen paws, there was no significant changes among ETN (8 paws), MTX (7 paws) and vehicle (5 paws) treated paws. (D) Delta arthritis score values were shown that no difference was found among ETN, MTX and vehicle treated paws. (E) In non-fully swollen paws, ETN treated paws (8 paws) decreased their arthritis scores, but MTX treated paws (9 paws) did not change their arthritis scores during the treatment. However, vehicle treated paws (3 paws) significantly increased their arthritis scores during the treatment. (F) Delta arthritis score values of ETN and MTX treated paws were lower than vehicle treated paws. Statistical significance was determined by Kruskal-Wallis test. *$p < 0.05$, **$p < 0.005$, ***$p < 0.0005$. Data presented are the means ± s.e.m.

(A) ETN treated group

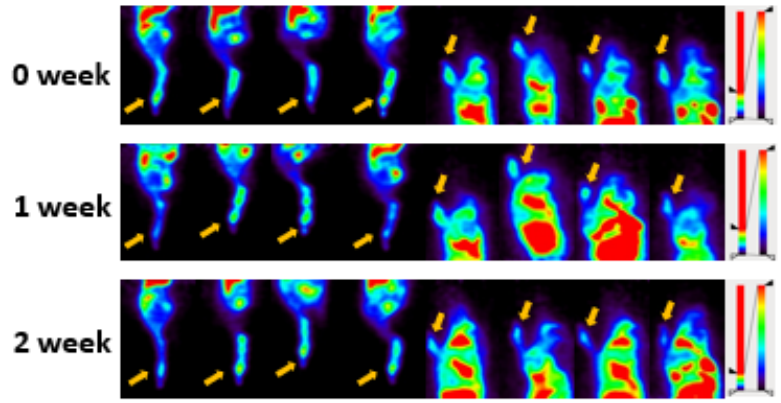

(B) MTX treated group

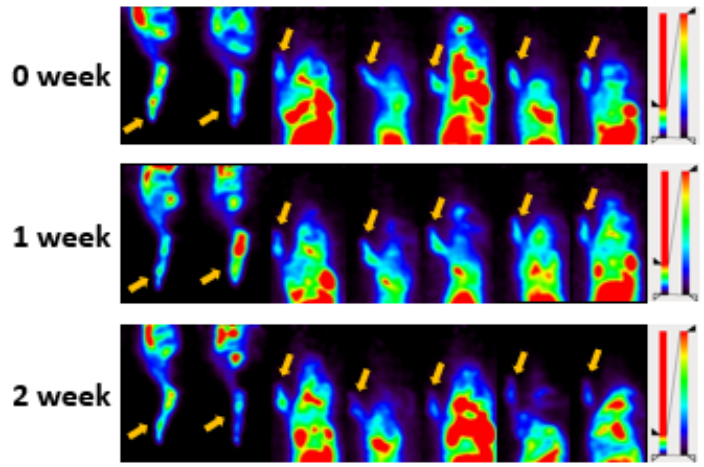

(B) Vehicle treated group

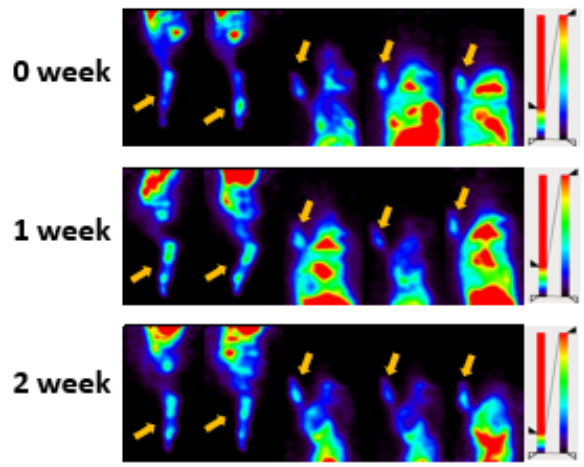

Figure 11. ^{18}F-FEDAC PET images in CIA mice after ETN, MTX or vehicle treatment

Representative ^{18}F-FEDAC PET images were shown. ^{18}F-FEDAC PET images were acquired pre-treatment of ETN, MTX or vehicle (0 week) and follow-up images were acquired at 1 and 2 weeks. (A) Paws of ETN, (B) MTX, and (C) vehicle treatment didn't show significant uptake changes in arthritic joints during the treatment. Orange allows indicate ^{18}F-FEDAC uptake in arthritic joints.

(A) ETN treated group

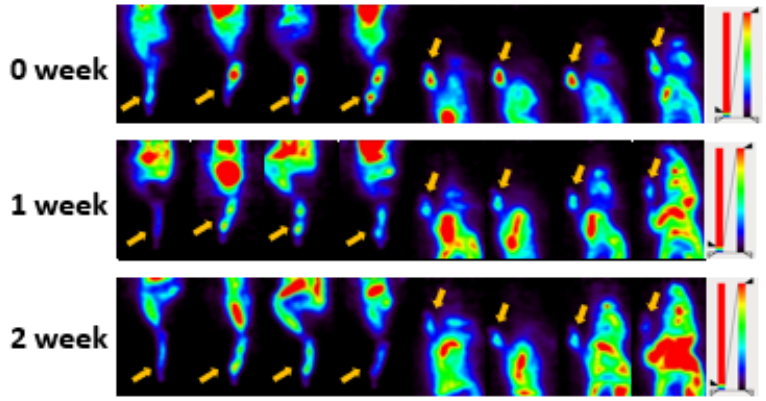

(B) MTX treated group

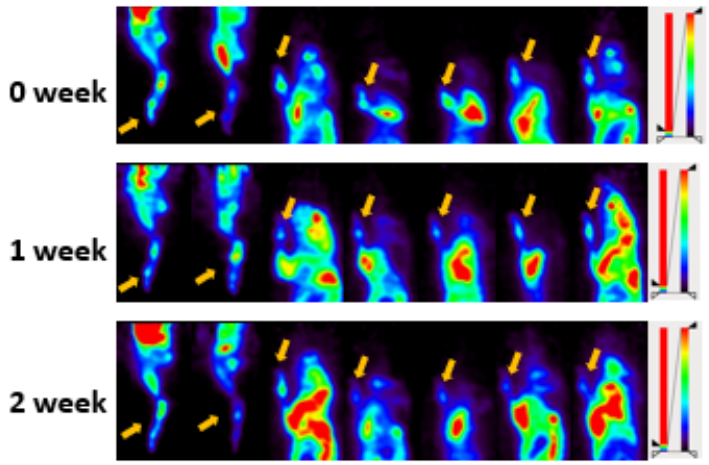

(B) Vehicle treated group

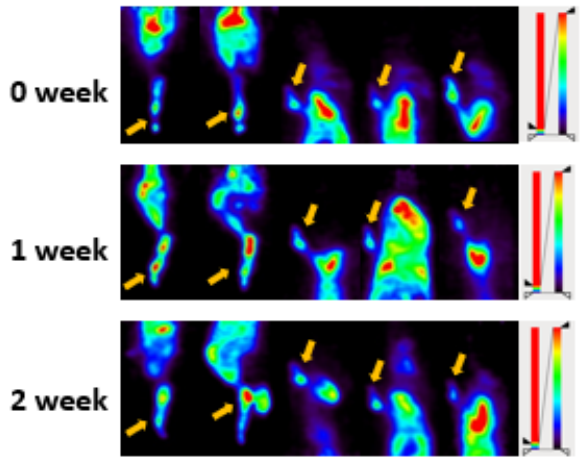

Figure 12. ^{18}F-FDG PET images in CIA mice after ETN, MTX or vehicle treatment

Representative ^{18}F-FDG PET images were shown. ^{18}F-FDG PET images in CIA mice were acquired pre-treatment of ETN, MTX or vehicle (0 week) and follow-up images were acquired at 1 and 2 weeks. (A) Paws of ETN and (B) paws of MTX treatment were significantly decreased their uptakes of ^{18}F-FDG during the treatment. However, (C) paws of vehicle treatment were not decreased their uptakes of ^{18}F-FDG during the treatment. Orange allows indicate ^{18}F-FDG uptake in arthritic joints.

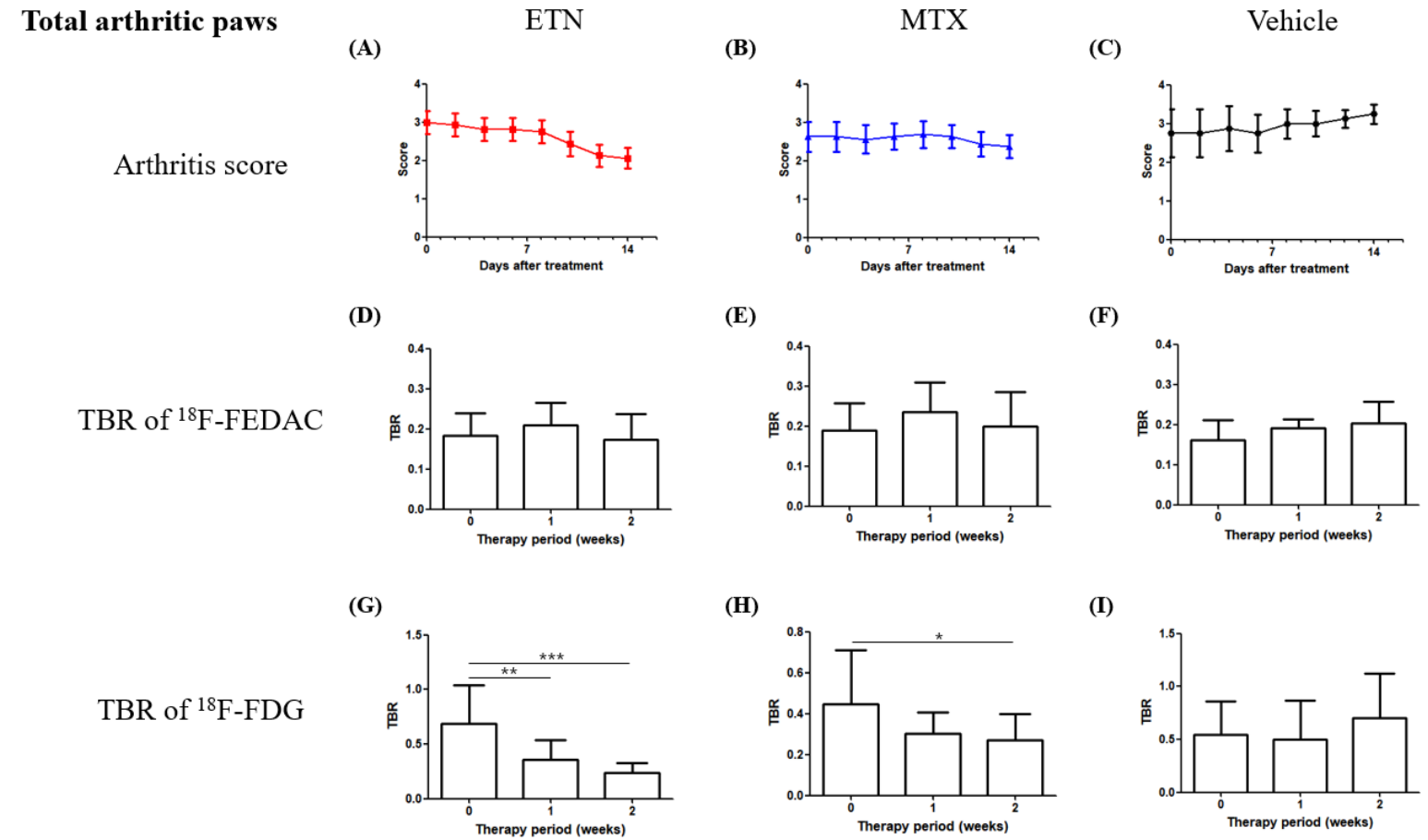
Total arthritic paws
ETN
MTX
Vehicle
(A)
(B)
(C)
Arthritis score
Score
Days after treatment
(D)
(E)
(F)
TBR of 18F-FEDAC
TBR
Therapy period (weeks)
(G)
(H)
(I)
TBR of 18F-FDG
***
**
*

Figure 13. Arthritis scores and TBR graphs of ^{18}F-FEDAC and ^{18}F-FDG PET in arthritic paws after ETN, MTX or vehicle treatment

In arthritis score graphs, (A) ETN (16 paws) and (B) MTX (16 paws) treated paws slightly decreased during the treatment, but (C) vehicle (8 paws) treated paws slightly increased during the treatment. In ^{18}F-FEDAC PET scans, TBR values of (D) ETN, (E) MTX and (F) vehicle treated paws did not change during the treatment. In ^{18}F-FDG PET scans, TBR values of (G) ETN and (H) MTX treated paws decreased during the treatment. However, TBR values of (I) vehicle treated paws did not change during the treatment. Statistical significance was determined by Mann-Whitney test. *$p < 0.05$, **$p < 0.005$, ***$p < 0.0005$. Data presented are the means ± s.e.m. in arthritis score graphs and data presented are the means ± s.d. in TBR graphs.

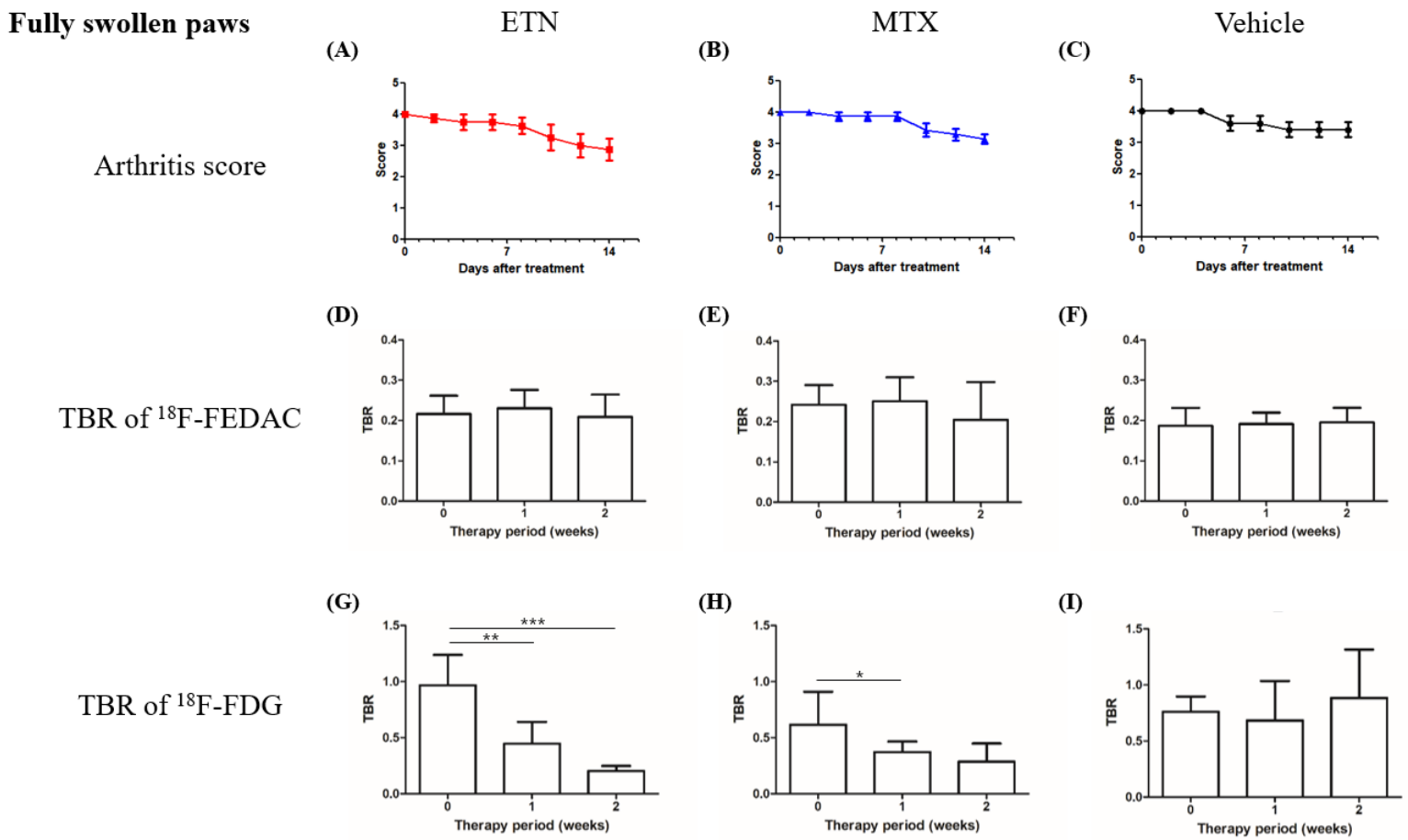
Fully swollen paws
ETN
MTX
Vehicle
(A)
(B)
(C)
Arthritis score
Score
Days after treatment
(D)
(E)
(F)
TBR of 18F-FEDAC
TBR
Therapy period (weeks)
(G)
(H)
(I)
TBR of 18F-FDG
***
**
*

Figure 14. Arthritis scores and TBR graphs of ^{18}F-FEDAC and ^{18}F-FDG PET in fully swollen paws after ETN, MTX or vehicle treatment

In arthritis score graphs, (A) ETN (8 paws), (B) MTX (7 paws) and (C) vehicle (5 paws) treated paws slightly decreased during the treatment. In ^{18}F-FEDAC PET scans, TBR values of (D) ETN, (E) MTX and (F) vehicle treated paws did not change during the treatment. In ^{18}F-FDG PET scans, TBR values of (G) ETN and (H) MTX treated paws decreased during the treatment. However, TBR values of (I) vehicle treated paws did not change during the treatment. Statistical significance was determined by Mann-Whitney test. *$p < 0.05$, **$p < 0.005$, ***$p < 0.0005$. Data presented are the means ± s.e.m. in arthritis score graphs and data presented are the means ± s.d. in TBR graphs.

Non-fully swollen paws

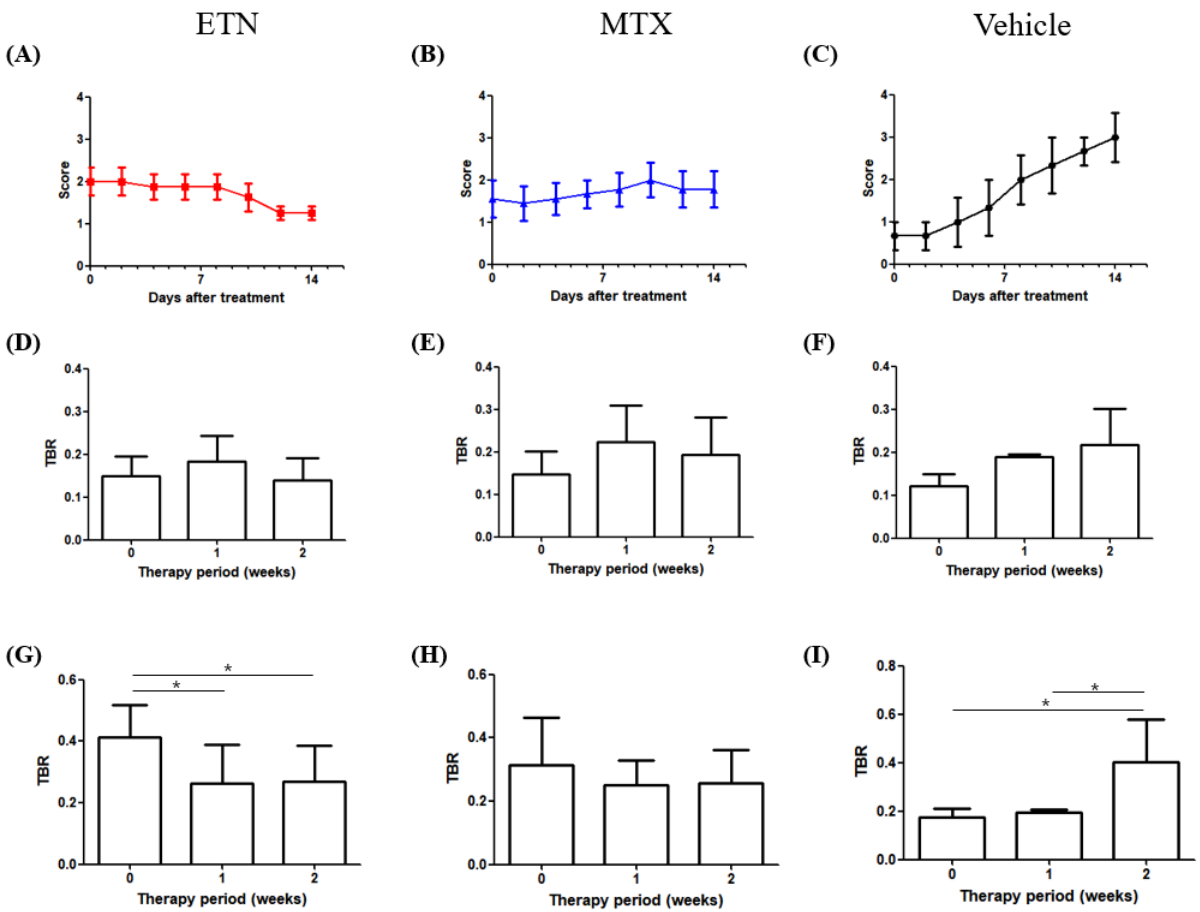

Figure 15. Arthritis scores and TBR graphs of ^{18}F-FEDAC and ^{18}F-FDG PET in non-fully swollen paws after ETN, MTX or vehicle treatment

In arthritis score graphs, (A) ETN (8 paws) treated paws decreased and (B) MTX (9 paws) treated paws did not decreased during the treatment. (C) Vehicle (3 paws) treated paws significantly increased their arthritis scores during the treatment. In ^{18}F-FEDAC PET scans, TBR values of (D) ETN, (E) MTX and (F) vehicle treated paws did not change during the treatment. In ^{18}F-FDG PET scans, TBR values of (G) ETN treated paws decreased during the treatment, but (H) MTX treated paws did not decrease during the treatment. In contrast, TBR values of (I) vehicle treated paws increased during the treatment. Statistical significance was determined by Mann-Whitney test. *$p < 0.05$. Data presented are the means ± s.e.m. in arthritis score graphs and data presented are the means ± s.d. in TBR graphs.

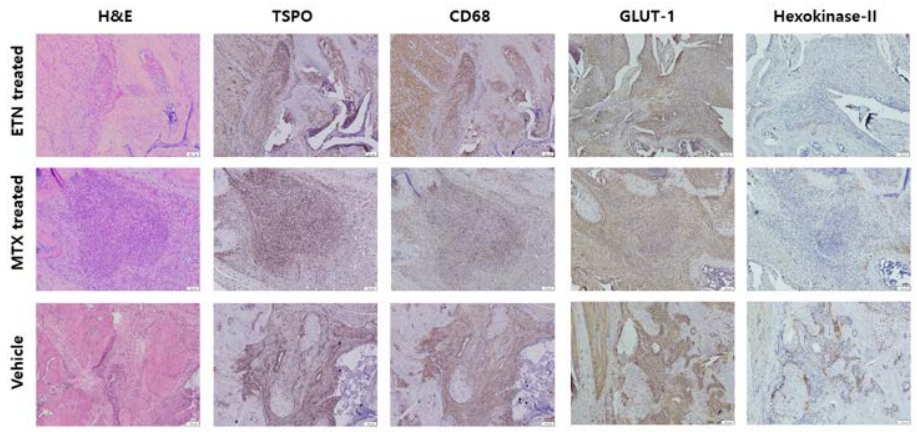

Figure 16. Immunohistochemistry of TSPO, CD68, GLUT-1 and hexokinase-II in arthritic joint tissues after ETN, MTX or vehicle treatment

Representative arthritic joint tissue images of H&E and immunostaining with TSPO, CD68, GLUT-1 and hexokinase-II were shown. Infiltrated cells were found in arthritic joints of ENT, MTX or vehicle treatment. Both TSPO and CD68 were colocalized in infiltrated cells. The expression of GLUT-1 was found in joint tissues with ETN and MTX treatment. However, the expression of hexokinase-II was not found in joint tissues with ETN and MTX treatment compared to vehicle treatment. We used three different paws of each treatment group of ETN, MTX or vehicle for the confirmation.

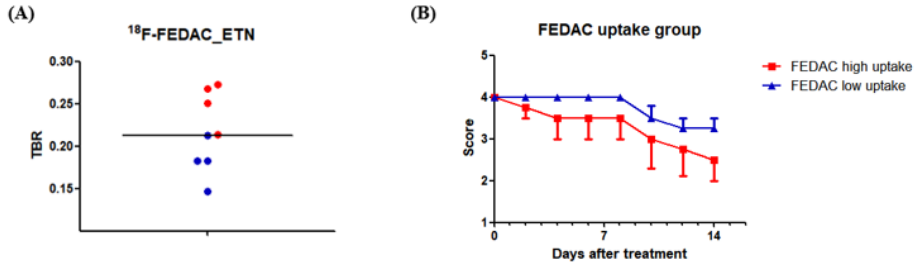

Figure 17. Arthritis score graphs between high and low tracer uptake group in ETN treated CIA mice

(A) Based on TBR values pre-treatment of ETN, joints were divided into high (red dot) and low FEDAC uptake group (blue dot) according to the median TBR value (vertical axis dotted). (B) The pattern of arthritis score was showed both in FEDAC high and FEDAC low uptake group. FEDAC high uptake group showed more decreased pattern than FEDAC low uptake group. Data presented are the means ± s.e.m.

DISCUSSION

In previous study, we found that ^{18}F-FEDAC was useful in monitoring activated macrophages (Fig. 1). Also, ^{18}F-FEDAC can be used to visualize arthritic joints in early stages (Fig. 2) (55). ^{18}F-FEDAC uptake increased in the joints of CIA mice on early phase (on day 23), although no clinical signs of arthritis. In contrast, ^{18}F-FDG uptake did not increase in the joints of CIA mice on early phase. On late phase (on day 37), ^{18}F-FDG uptake increased along with the deterioration of clinical arthritis (Table 1). From these results, we suggest that ^{18}F-FEDAC is reliable tracer to detect activated macrophages in RA model, even in the early phase of active inflammation.

At the first step, we tried to monitor the therapeutic response of TNF-antagonist (ETN) in CIA mouse model. Arthritis scores decreased in arthritic paws during ETN treatment (100 μg) (57, 58). In fully swollen paws, arthritis scores did not significantly decrease compared to non-fully swollen paws. In non-fully swollen paws, arthritis scores significantly decreased in arthritic paws

during ETN treatment. Therefore, we confirmed that ETN showed therapeutic effect in CIA mice.

TNF-α is one of the important proinflammatory cytokines in RA pathogenesis and activates non-stimulated macrophages (59). Most proinflammatory cytokines like IL-1 and TNF-α in pannus are released by activated macrophages (60). Therefore, we assumed that ^{18}F-FEDAC could monitor therapeutic response of TNF-antagonist (ETN). As a basic data, we found that translocations of NF-κB in nucleus decreased after ETN treatment by immunofluorescence staining. This finding meant that ETN inhibited TNF based activation pathway of macrophages. In our data, the expression of TSPO and ^{18}F-FEDAC cell uptakes did not change during the ETN treatment in activated macrophages. In CIA mice, arthritis scores gradually decreased during ETN treatment compared to vehicle treatment. However, ^{18}F-FEDAC uptake in inflamed paws did not change during the ETN treatment. Also, immunostaining results showed that the number of activated macrophages was similar between ETN and vehicle treated joints. This result showed that ETN

didn't influence the TSPO expression in macrophages which already activated. In addition, the number of activated macrophages was unchangeable during the ETN treatment in CIA mice. We found that ^{18}F-FEDAC was not suitable to monitor ETN therapeutic response in CIA mice.

The results were similar with the MTX treatment in RA models. We used MTX as a nonspecific cytotoxic agent to activated macrophages comparing to ETN. MTX is a folic acid antagonist which competitively inhibits dihydrofolate reductase (DHFR) to disrupt cellular folate metabolism (61). In addition, it has not only cytotoxicity effect but also immunomodulatory function in low-dose treatment. We used low-dose MTX both *in vitro* and *in vivo* experiments. The expression of TSPO and ^{18}F-FEDAC cell uptakes did not change during the MTX treatment in activated macrophages. In CIA mice, arthritis scores did not decrease during the MTX treatment. ^{18}F-FEDAC uptakes in CIA inflamed paws didn't change during the MTX treatment. Immunostaining results showed that the number of activated macrophages were similar between MTX and vehicle treated joints. Both ETN and MTX treatment

groups showed similar ^{18}F-FEDAC accumulation *in vitro* and *in vivo*. Neither ETN nor MTX did influence the TSPO expression in macrophages which have already been activated. From these results, we can speculate that TSPO can be used as a signature marker for rheumatoid arthritis occurrence, even after therapeutic interventions.

We compared ^{18}F-FDG PET scan and ^{18}F-FEDAC PET scan in therapeutic response. ^{18}F-FDG uptake in inflammation site is known to reflect cell proliferation and glucose metabolic changes of all kind of inflammatory cells (62-64). The expressions of GLUT-1 and hexokinase-II, which are known as glucose transporter and enzyme to produce glucose-6-phosphate, are known to be the most important for ^{18}F-FDG uptake (65-68). In cellular level, the expression of GLUT-1 and hexokinase-II didn't significantly change after ETN or MTX treatment. ^{18}F-FDG uptake decreased during the ETN treatment but the magnitude of decrease is less than 15%. However, ^{18}F-FDG uptakes in CIA mice decreased significantly during the ETN or MTX treatment rather than vehicle treated CIA mice (non-therapy group). Especially in fully swollen paws,

ETN and MTX treated paws showed significantly decreased ^{18}F-FDG accumulation, even if their arthritis scores did not decrease after ETN or MTX treatment. We can speculate that ^{18}F-FDG PET can be an early predictive tracer of treatment response compared to arthritis score. In immunostaining results showed that GLUT-1 expression was similar but hexokinase-II expression was more downregulated in ETN or MTX treated joints than vehicle treated joint. Anti-inflammatory effect of ETN or MTX subsequently decrease activity of whole inflammatory cells in inflamed paws resulting decreased ^{18}F-FDG accumulation.

Although ^{18}F-FDG was more reliable to monitor therapy response, ^{18}F-FDG had a limitation in detection of early stage of RA (55). In contrast, ^{18}F-FEDAC uptake increased in the joints of CIA mice on early phase. In addition, there was chance to use TSPO as a predictive marker for therapeutic response of TNF-antagonist. In a limited number of CIA mice, we divided joints according to the ^{18}F-FEDAC uptakes pre-treatment of ETN (Fig. 17a). The joints of high ^{18}F-FEDAC uptake showed significant decrease pattern of

arthritis scores to ETN treatment compared to those of low ^{18}F-FEDAC uptake (Fig. 17b). From this result, the joints of high ^{18}F-FEDAC uptake may show more sensitivity to ETN treatment than low ^{18}F-FEDAC uptake. However, this result did not reach the statistical significancy, which may be caused by the reason of the insufficient number of arthritic joints evaluated. Therefore, we need additional study of TSPO targeting PET ligand as a predictive role in therapeutic response to TNF-antagonist.

There were some limitations in our study. First, we didn't confirm that ^{18}F-FEDAC actually bound to activated macrophages in arthritic joints. Alternatively, we found that TSPO and macrophages were colocalized in inflamed arthritic tissues. Second, we just treated ETN and MTX no longer than two weeks for therapeutic response. ^{18}F-FEDAC uptakes may be changeable after long-term therapy. Additional study is needed in the TSPO expression change for the long-term therapeutic response. Third, we did not design our experiment initially in order for the evaluation of the possibility of TSPO as a predictive marker. Even though there was a tendency of different response in

bDMARDs according to the TSPO expression only in response experimental model, we had not enough number of arthritis joints to confirm the usefulness of TSPO as a predictive marker. Therefore, another experiments with a well-designed for prediction of response is needed to the conclusion. We used MTX as a control of nonspecific medication. MTX may directly affect anti-inflammatory action to inflammatory cells including activated macrophages (61).

In conclusion, ^{18}F-FEDAC PET can image inflamed joint by targeting overexpressed TSPO of activated macrophages in CIA mice. However, ^{18}F-FEDAC had a limited role to evaluate the therapeutic response by ETN. ^{18}F-FEDAC uptake of arthritic joint did not change during ETN treatment. We found similar phenomenon in *in vitro* cell study, that is no change of ^{18}F-FEDAC uptake in macrophages after drugs treatment. Sustained TSPO expression was found once after activation in macrophages. According to the characteristic of TSPO expression, ^{18}F-FEDAC may be used as a signature marker for activated macrophages during the course of rheumatoid arthritis,

even after therapeutic interventions. In contrast, ^{18}F-FDG PET was shown to have more reliable results to monitor therapeutic response of ETN treatment than ^{18}F-FEDAC PET. ^{18}F-FDG PET may be expected as an imaging biomarker to monitor therapeutic response of RA.

REFERENCES

1. Gabriel SE. The epidemiology of rheumatoid arthritis. Rheum Dis Clin North Am. 2001;27(2):269-81.

2. Firestein GS. Evolving concepts of rheumatoid arthritis. Nature. 2003;423(6937):356-61.

3. Pincus T, Callahan LF, Sale WG, Brooks AL, Payne LE, Vaughn WK. Severe functional declines, work disability, and increased mortality in seventy-five rheumatoid arthritis patients studied over nine years. Arthritis Rheum. 1984;27(8):864-72.

4. Wolfe F, Mitchell DM, Sibley JT, Fries JF, Bloch DA, Williams CA, et al. The mortality of rheumatoid arthritis. Arthritis Rheum. 1994;37(4):481-94.

5. Harris ED, Jr. Rheumatoid arthritis. Pathophysiology and implications for therapy. N Engl J Med. 1990;322(18):1277-89.

6. Curtis JR, Xi J, Patkar N, Xie A, Saag KG, Martin C. Drug-specific and time-dependent risks of bacterial infection among patients with rheumatoid arthritis who were exposed to tumor necrosis factor alpha antagonists. Arthritis Rheum. 2007;56(12):4226-7.

7. Gaffo A, Saag KG, Curtis JR. Treatment of rheumatoid arthritis. Am J Health Syst Pharm. 2006;63(24):2451-65.

8. Weinblatt ME, Coblyn JS, Fox DA, Fraser PA, Holdsworth DE, Glass DN, et al. Efficacy of low-dose methotrexate in rheumatoid arthritis. N Engl J Med. 1985;312(13):818-22.

9. Williams HJ, Willkens RF, Samuelson CO, Jr., Alarcon GS, Guttadauria M, Yarboro C, et al. Comparison of low-dose oral pulse methotrexate and placebo in the treatment of rheumatoid arthritis. A controlled clinical trial. Arthritis Rheum. 1985;28(7):721-30.

10. Weinblatt ME, Weissman BN, Holdsworth DE, Fraser PA, Maier AL, Falchuk KR, et al. Long-term prospective study of methotrexate in the treatment of rheumatoid arthritis. 84-month update. Arthritis Rheum. 1992;35(2):129-37.

11. Hu SK, Mitcho YL, Oronsky AL, Kerwar SS. Studies on the effect of methotrexate on macrophage function. J Rheumatol. 1988;15(2):206-9.

12. Sperling RI, Benincaso AI, Anderson RJ, Coblyn JS, Austen KF, Weinblatt ME. Acute and chronic suppression of leukotriene B4 synthesis ex vivo in neutrophils from patients with rheumatoid arthritis beginning treatment

with methotrexate. Arthritis Rheum. 1992;35(4):376-84.

13. Atzinger CB, Guo JJ. Biologic disease-modifying antirheumatic drugs in a national, privately insured population: utilization, expenditures, and price trends. Am Health Drug Benefits. 2017;10(1):27-36.

14. Cash JM, Klippel JH. Second-line drug therapy for rheumatoid arthritis. N Engl J Med. 1994;330(19):1368-75.

15. McInnes IB, Schett G. Cytokines in the pathogenesis of rheumatoid arthritis. Nat Rev Immunol. 2007;7(6):429-42.

16. Smolen JS, Aletaha D, Koeller M, Weisman MH, Emery P. New therapies for treatment of rheumatoid arthritis. Lancet. 2007;370(9602):1861-74.

17. Curtis JR, Singh JA. Use of biologics in rheumatoid arthritis: current and emerging paradigms of care. Clin Ther. 2011;33(6):679-707.

18. Sokka T, Hannonen P, Mottonen T. Conventional disease-modifying antirheumatic drugs in early arthritis. Rheum Dis Clin North Am. 2005;31(4):729-44.

19. Sokka T, Envalds M, Pincus T. Treatment of rheumatoid arthritis: a

global perspective on the use of antirheumatic drugs. Mod Rheumatol. 2008;18(3):228-39.

20. Rosado-de-Castro PH, Lopes de Souza SA, Alexandre D, Barbosa da Fonseca LM, Gutfilen B. Rheumatoid arthritis: nuclear medicine state-of-the-art imaging. World J Orthop. 2014;5(3):312-8.

21. Brown AK, Wakefield RJ, Conaghan PG, Karim Z, O'Connor PJ, Emery P. New approaches to imaging early inflammatory arthritis. Clin Exp Rheumatol. 2004;22(5 Suppl 35):S18-25.

22. Boutry N, Morel M, Flipo RM, Demondion X, Cotten A. Early rheumatoid arthritis: a review of MRI and sonographic findings. AJR Am J Roentgenol. 2007;189(6):1502-9.

23. Freeston JE, Bird P, Conaghan PG. The role of MRI in rheumatoid arthritis: research and clinical issues. Curr Opin Rheumatol. 2009;21(2):95-101.

24. Narvaez JA, Narvaez J, De Lama E, De Albert M. MR imaging of early rheumatoid arthritis. Radiographics. 2010;30(1):143-63; discussion 63-5.

25. McQueen FM, Stewart N, Crabbe J, Robinson E, Yeoman S, Tan PL, et al. Magnetic resonance imaging of the wrist in early rheumatoid arthritis reveals a high prevalence of erosions at four months after symptom onset. Ann

Rheum Dis. 1998;57(6):350-6.

26. Lindegaard H, Vallo J, Horslev-Petersen K, Junker P, Ostergaard M. Low field dedicated magnetic resonance imaging in untreated rheumatoid arthritis of recent onset. Ann Rheum Dis. 2001;60(8):770-6.

27. Ostergaard M, Ejbjerg B, Szkudlarek M. Imaging in early rheumatoid arthritis: roles of magnetic resonance imaging, ultrasonography, conventional radiography and computed tomography. Best Pract Res Clin Rheumatol. 2005;19(1):91-116.

28. Dill T. Contraindications to magnetic resonance imaging: non-invasive imaging. Heart. 2008;94(7):943-8.

29. Link TM. Osteoporosis imaging: state of the art and advanced imaging. Radiology. 2012;263(1):3-17.

30. Wunder A, Straub RH, Gay S, Funk J, Muller-Ladner U. Molecular imaging: novel tools in visualizing rheumatoid arthritis. Rheumatology (Oxford). 2005;44(11):1341-9.

31. Pichler BJ, Wehrl HF, Judenhofer MS. Latest advances in molecular imaging instrumentation. J Nucl Med. 2008;49 Suppl 2:5S-23S.

32. Zeman MN, Scott PJ. Current imaging strategies in rheumatoid arthritis. Am J Nucl Med Mol Imaging. 2012;2(2):174-220.

33. Backhaus M, Kamradt T, Sandrock D, Loreck D, Fritz J, Wolf KJ, et al. Arthritis of the finger joints: a comprehensive approach comparing conventional radiography, scintigraphy, ultrasound, and contrast-enhanced magnetic resonance imaging. Arthritis Rheum. 1999;42(6):1232-45.

34. Wu C, Li F, Niu G, Chen X. PET imaging of inflammation biomarkers. Theranostics. 2013;3(7):448-66.

35. Bakheet SM, Saleem M, Powe J, Al-Amro A, Larsson SG, Mahassin Z. F-18 fluorodeoxyglucose chest uptake in lung inflammation and infection. Clin Nucl Med. 2000;25(4):273-8.

36. van Waarde A, Cobben DC, Suurmeijer AJ, Maas B, Vaalburg W, de Vries EF, et al. Selectivity of ^{18}F-FLT and ^{18}F-FDG for differentiating tumor from inflammation in a rodent model. J Nucl Med. 2004;45(4):695-700.

37. Zhuang H, Alavi A. 18-fluorodeoxyglucose positron emission tomographic imaging in the detection and monitoring of infection and inflammation. Semin Nucl Med. 2002;32(1):47-59.

38. Paik JY, Lee KH, Choe YS, Choi Y, Kim BT. Augmented ^{18}F-FDG

uptake in activated monocytes occurs during the priming process and involves tyrosine kinases and protein kinase C. J Nucl Med. 2004;45(1):124-8.

39. Yamada S, Kubota K, Kubota R, Ido T, Tamahashi N. High accumulation of fluorine-18-fluorodeoxyglucose in turpentine-induced inflammatory tissue. J Nucl Med. 1995;36(7):1301-6.

40. Selvaraj V, Tu LN. Current status and future perspectives: TSPO in steroid neuroendocrinology. J Endocrinol. 2016;231(1):R1-R30.

41. Papadopoulos V, Baraldi M, Guilarte TR, Knudsen TB, Lacapere JJ, Lindemann P, et al. Translocator protein (18kDa): new nomenclature for the peripheral-type benzodiazepine receptor based on its structure and molecular function. Trends Pharmacol Sci. 2006;27(8):402-9.

42. van der Laken CJ, Elzinga EH, Kropholler MA, Molthoff CF, van der Heijden JW, Maruyama K, et al. Noninvasive imaging of macrophages in rheumatoid synovitis using ^{11}C-(R)-PK11195 and positron emission tomography. Arthritis Rheum. 2008;58(11):3350-5.

43. Gent YY, Voskuyl AE, Kloet RW, van Schaardenburg D, Hoekstra OS, Dijkmans BA, et al. Macrophage positron emission tomography imaging as a biomarker for preclinical rheumatoid arthritis: findings of a prospective pilot study. Arthritis Rheum. 2012;64(1):62-6.

44. Gent YY, Weijers K, Molthoff CF, Windhorst AD, Huisman MC, Kassiou M, et al. Promising potential of new generation translocator protein tracers providing enhanced contrast of arthritis imaging by positron emission tomography in a rat model of arthritis. Arthritis Res Ther. 2014;16(2):R70.

45. Gulyas B, Makkai B, Kasa P, Gulya K, Bakota L, Varszegi S, et al. A comparative autoradiography study in post mortem whole hemisphere human brain slices taken from Alzheimer patients and age-matched controls using two radiolabelled DAA1106 analogues with high affinity to the peripheral benzodiazepine receptor (PBR) system. Neurochem Int. 2009;54(1):28-36.

46. Takashima-Hirano M, Shukuri M, Takashima T, Goto M, Wada Y, Watanabe Y, et al. General method for the ^{11}C-labeling of 2-arylpropionic acids and their esters: construction of a PET tracer library for a study of biological events involved in COXs expression. Chemistry. 2010;16(14):4250-8.

47. Oh U, Fujita M, Ikonomidou VN, Evangelou IE, Matsuura E, Harberts E, et al. Translocator protein PET imaging for glial activation in multiple sclerosis. J Neuroimmune Pharmacol. 2011;6(3):354-61.

48. Price GW, Ahier RG, Hume SP, Myers R, Manjil L, Cremer JE, et al. In vivo binding to peripheral benzodiazepine binding sites in lesioned rat brain: comparison between [^{3}H]PK11195 and [^{18}F]PK14105 as markers for neuronal

damage. J Neurochem. 1990;55(1):175-85.

49. Callaghan PD, Wimberley CA, Rahardjo GL, Berghofer PJ, Pham TQ, Jackson T, et al. Comparison of in vivo binding properties of the 18-kDa translocator protein (TSPO) ligands [^{18}F]PBR102 and [^{18}F]PBR111 in a model of excitotoxin-induced neuroinflammation. Eur J Nucl Med Mol Imaging. 2015;42(1):138-51.

50. Perrone M, Moon BS, Park HS, Laquintana V, Jung JH, Cutrignelli A, et al. A Novel PET imaging probe for the detection and monitoring of translocator protein 18 kDa expression in pathological disorders. Sci Rep. 2016;6:20422.

51. Moon BS, Kim BS, Park C, Jung JH, Lee YW, Lee HY, et al. [^{18}F]Fluoromethyl-PBR28 as a potential radiotracer for TSPO: preclinical comparison with [^{11}C]PBR28 in a rat model of neuroinflammation. Bioconjug Chem. 2014;25(2):442-50.

52. Yanamoto K, Kumata K, Yamasaki T, Odawara C, Kawamura K, Yui J, et al. [^{18}F]FEAC and [^{18}F]FEDAC: Two novel positron emission tomography ligands for peripheral-type benzodiazepine receptor in the brain. Bioorg Med Chem Lett. 2009;19(6):1707-10.

53. Yui J, Maeda J, Kumata K, Kawamura K, Yanamoto K, Hatori A, et al.

^{18}F-FEAC and ^{18}F-FEDAC: PET of the monkey brain and imaging of translocator protein (18 kDa) in the infarcted rat brain. J Nucl Med. 2010;51(8):1301-9.

54. Hatori A, Yui J, Yamasaki T, Xie L, Kumata K, Fujinaga M, et al. PET imaging of lung inflammation with [^{18}F]FEDAC, a radioligand for translocator protein (18 kDa). PLoS One. 2012;7(9):e45065.

55. Chung SJ, Yoon HJ, Youn H, Kim MJ, Lee YS, Jeong JM, et al. ^{18}F-FEDAC as a targeting agent for activated macrophages in DBA/1 mice with collagen-induced arthritis: comparison with ^{18}F-FDG. J Nucl Med. 2018;59(5):839-45.

56. Brand DD, Latham KA, Rosloniec EF. Collagen-induced arthritis. Nat Protoc. 2007;2(5):1269-75.

57. Wang QT, Wu YJ, Huang B, Ma YK, Song SS, Zhang LL, et al. Etanercept attenuates collagen-induced arthritis by modulating the association between BAFFR expression and the production of splenic memory B cells. Pharmacol Res. 2013;68(1):38-45.

58. Yi H, Kim J, Jung H, Rim YA, Kim Y, Jung SM, et al. Induced production of anti-etanercept antibody in collagen-induced arthritis. Mol Med Rep. 2014;9(6):2301-8.

59. Choy EH, Panayi GS. Cytokine pathways and joint inflammation in rheumatoid arthritis. N Engl J Med. 2001;344(12):907-16.

60. Kavanaugh AF, Schulze-Koops H, Davis LS, Lipsky PE. Repeat treatment of rheumatoid arthritis patients with a murine anti-intercellular adhesion molecule 1 monoclonal antibody. Arthritis Rheum. 1997;40(5):849-53.

61. Fotoohi AK, Albertioni F. Mechanisms of antifolate resistance and methotrexate efficacy in leukemia cells. Leuk Lymphoma. 2008;49(3):410-26.

62. Cher LM, Murone C, Lawrentschuk N, Ramdave S, Papenfuss A, Hannah A, et al. Correlation of hypoxic cell fraction and angiogenesis with glucose metabolic rate in gliomas using ^{18}F-fluoromisonidazole, ^{18}F-FDG PET, and immunohistochemical studies. J Nucl Med. 2006;47(3):410-8.

63. Riedl CC, Akhurst T, Larson S, Stanziale SF, Tuorto S, Bhargava A, et al. ^{18}F-FDG PET scanning correlates with tissue markers of poor prognosis and predicts mortality for patients after liver resection for colorectal metastases. J Nucl Med. 2007;48(5):771-5.

64. Takenaka T, Yano T, Ito K, Morodomi Y, Miura N, Kawano D, et al. Biological significance of the maximum standardized uptake values on positron

emission tomography in non-small cell lung cancer. J Surg Oncol. 2009;100(8):688-92.

65. Younes M, Lechago LV, Somoano JR, Mosharaf M, Lechago J. Wide expression of the human erythrocyte glucose transporter Glut1 in human cancers. Cancer Res. 1996;56(5):1164-7.

66. Ito T, Noguchi Y, Satoh S, Hayashi H, Inayama Y, Kitamura H. Expression of facilitative glucose transporter isoforms in lung carcinomas: its relation to histologic type, differentiation grade, and tumor stage. Mod Pathol. 1998;11(5):437-43.

67. Kurata T, Oguri T, Isobe T, Ishioka S, Yamakido M. Differential expression of facilitative glucose transporter (GLUT) genes in primary lung cancers and their liver metastases. Jpn J Cancer Res. 1999;90(11):1238-43.

68. Mathupala SP, Rempel A, Pedersen PL. Aberrant glycolytic metabolism of cancer cells: a remarkable coordination of genetic, transcriptional, post-translational, and mutational events that lead to a critical role for type II hexokinase. J Bioenerg Biomembr. 1997;29(4):339-43.

국문초록

서론: 류마티스 관절염은 염증에 의한 관절 및 뼈의 손상을 가져오는 자가면역 질환 중 하나이다. 활성 대식세포는 류마티스 관절염 발생 중에 중요한 역할을 하고 있으며, 생물학적 항류마티스 제제에 의하여 치료가 가능하다. ^{18}F-FEDAC은 활성 대식세포에서 과량 발현되는 전이체 단백질(TSPO; translocator protein)을 표적으로 하는 추적자이다. 이전 연구에서 우리는 TSPO 표적 추적자인 ^{18}F-FEDAC을 이용한 양전자단층촬영법(Positron Emission Tomography; PET)으로 류마티스 관절염 동물 모델에서 활성 대식세포를 비침습적으로 확인할 수 있었다. 이번 연구에서는 류마티스 관절염 동물 모델에서 생물학적 항류마티스 제제인 TNF 길항제를 사용시, 치료 전후의 ^{18}F-FEDAC 섭취 변화를 임상 및 실험 지표와 비교연구하였다.

방법: 세포 수준의 실험에 사용할 ETN(etanercept; 생물학적 항류마티스 제제)과 MTX(methotrexate)의 농도를 결정하기 위하여 마우스 대식세포주인 RAW 264.7 세포에서 CCK-8 실험을 진행하였다. 세포들은 LPS와 IFN-γ를 이용하여 활

성화된 상태로 유도하였다. Western blotting을 통하여 약물 처리 전후의 TSPO와 당 섭취관련 단백질(GLUT-1, hexokinase-II)의 발현 변화와 ^{18}F-FEDAC, ^{18}F-FDG 세포 섭취를 비교하였다. 동물 실험으로 DBA1 마우스에 adjuvant와 제2형 콜라겐의 혼합물을 피하 주사하여 만든 콜라겐 유도 관절염(collagen-induced arthritis; CIA) 마우스 모델을 사용하였다. 관절염이 유도된 CIA 마우스들은 ETN, MTX, 식염수를 복강주사로 투여하였으며, 투여 후 주 1회씩 2주 동안 ^{18}F-FEDAC와 ^{18}F-FDG PET 영상을 촬영하였다. 실험이 종료된 후, 마우스 발조직을 면역염색 하였다.

결과: 활성화된 RAW 264.7 세포에서 TSPO 발현은 ETN과 MTX 처리 중에 변화가 없었고 GLUT-1, hexokinase-II의 발현 또한 변화가 없었다. 세포섭취 실험에서도 ^{18}F-FEDAC와 ^{18}F-FDG의 섭취는 ETN 또는 MTX 처리 중에 큰 변화가 없었다. CIA 마우스에서 ETN 또는 MTX 처리 시 ^{18}F-FEDAC PET 영상에서는 염증 관절의 섭취가 변하지 않았지만, ^{18}F-FDG PET 영상에서는 섭취가 감소하였다. 면역조직염색에서는 ETN 또는 MTX 처리한 조직 모두에서 TSPO, CD68, GLUT-1의 발현이 식염수 처리 조직과 비슷하였지만,

hexokinase-II 발현은 식염수 처리 조직에 비하여 현저히 낮아졌다.

결론: ^{18}F-FEDAC PET으로 CIA 마우스의 염증 관절에서 활성 대식세포 추적영상을 얻었을 수 있었다. 하지만 대식세포의 활성화 이후, TSPO가 지속적으로 발현되기 때문에 ^{18}F-FEDAC을 이용하여 치료 반응을 평가할 수 없었다. 이러한 TSPO의 발현 특징을 이용하면 ^{18}F-FEDAC PET은 RA 발현 과정에서 대식세포의 signature marker로 사용할 수 있을 것으로 생각된다. ^{18}F-FDG PET은 ETN 치료에 따라 염증 관절의 섭취가 감소되어 류마티스 관절염의 치료효과를 확인하는데 사용할 수 있을 것으로 생각된다.

주요어: 류마티스 관절염, 대식세포, 전이체 단백질, 양전자단층촬영법, 생물학적 항류마티스 제제, ^{18}F-FEDAC, ^{18}F-FDG

학번: 2014-22028